



Simulating regional impacts of irrigation on the atmospheric and terrestrial water cycle using Earth System Model physics

Pierre Tiengou^{1,2}, Agnès Ducharne¹, and Frédérique Cheruy²

¹METIS, IPSL, Sorbonne Université/CNRS/EPHE-PSL

²Laboratoire de Météorologie Dynamique, IPSL, Sorbonne Université/CNRS/École Normale Supérieure-PSL Research/Ecole Polytechnique-IPP, Paris, France

Correspondence: Pierre Tiengou (pierre.tiengou@sorbonne-universite.fr)

Abstract. This study presents regional simulations over the Iberian Peninsula between 2010 and 2022 with the atmospheric (ICOLMDZ) and land surface (ORCHIDEE) components of the IPSL climate model in a new limited area model configuration (25 km resolution). It uses a recently developed river routing and irrigation scheme based on a water-conservative supply-and-demand approach. Two simulations, with and without irrigation, are compared to isolate the impacts of simulated irrigation on land surface-atmosphere interactions and the water cycle. First, an evaluation of the simulations is conducted to characterize existing model biases in river discharge, precipitation and evapotranspiration (ET), and assess whether they can be improved by simulating irrigation. The simulated irrigation is too low in southern Spain because of a lack of available water in the reservoirs, and likely because of the absence of representation of river dams. In northern regions such as the Ebro Valley, the simulated irrigation is more realistic and reduces the biases of river discharge and ET in summer and autumn. Second, atmospheric changes induced by irrigation are studied in summer (JJA). Large atmospheric responses are found over intensely irrigated areas, mainly consisting of a shift in energy partitioning between the turbulent fluxes (increase in latent heat flux and decrease in sensible heat flux, up to 50 W m^{-2}), and a lowering of the atmospheric boundary layer (-100 m) and of the lifting condensation level (-250 m). Increases in precipitation are statistically significant only over the mountainous areas surrounding the Ebro Valley, and are closely linked to increases in convective available potential energy. Finally, atmospheric moisture recycling over the Iberian Peninsula is identified by showing that the increase in ET in the presence of irrigation exceeds the amount of water added by irrigation. This is made possible by an increase in precipitation over land, although most of this increase is located in lightly irrigated areas rather than in intensely irrigated areas. These results point to remote atmospheric effects of irrigation and motivate further investigation into surface-atmosphere coupling processes in the presence of irrigation in the IPSL model.



20 1 Introduction

Physical processes at the interface between the soil surface and the lower atmosphere can influence meteorological and hydrological variables at various spatial and temporal scales, contributing to complex feedback loops. In areas where the transition regime described by Budyko (1956); Budyko and Miller (1974) is most frequent, soil moisture (SM) plays a central role in these processes as a strong driver of evapotranspiration (ET), which conditions the partitioning of energy at the interface between
25 land and atmosphere (Betts and Ball, 1995; Seneviratne et al., 2010).

The GLACE experiment used general circulation models (GCMs) to identify regions of strong land surface-atmosphere coupling between SM and precipitation, which were mostly found in semiarid transition regions (Koster et al., 2004). This was confirmed by other modelling studies that also identified various mechanisms through which land surface conditions can impact the atmosphere in these coupling hotspots, and metrics to quantify them (Dirmeyer, 2011; Zou et al., 2023). Experiments
30 have also been implemented to isolate the response of the atmosphere to various surface conditions under a changing climate, such as GLACE-CMIP5 (Seneviratne et al., 2013) and have revealed that land-atmosphere coupling processes are a significant driver of the response of the water cycle to a global temperature rise in these hotspots (Berg et al., 2015). Moreover, some warm biases of the Coupled Model Intercomparison Project 5 (CMIP5) models (Christensen and Boberg, 2012; Mueller and Seneviratne, 2014) are linked to underestimates of SM (Al-Yaari et al., 2019) and were partly attributed to the representation
35 of land surface-atmosphere coupling processes (Cheruy et al., 2013, 2014), justifying ongoing research on their understanding and improvement within models.

A great source of complexity in land surface-atmosphere processes comes from the spatial heterogeneity of SM, which may be derived from the diversity of vegetation, soil types, orographic features, and anthropogenic processes. Increases in SM and ET have been associated with increases in precipitation in both modelling and observational studies (Koster et al., 2003;
40 Guo et al., 2006; Wei and Dirmeyer, 2012; Findell et al., 2011), constituting a positive feedback loop (moisture recycling, as presented in Eltahir and Bras, 1996). However, they can also lead to a stabilization of the atmospheric boundary layer (ABL), inhibiting vertical development and convection (Findell and Eltahir, 2003b; Ek and Holtslag, 2004). This leads to a negative feedback loop where convective rainfall is more likely to occur over drier soil patches. This negative spatial coupling was frequently noticed in observations (Taylor et al., 2012; Klein and Taylor, 2020), although Guillod et al. (2015) emphasized the
45 importance of temporal variability, showing that precipitation over drier soils occurs more often when soils are moister than usual at the regional scale. Finally, SM heterogeneities can affect precipitation through mesoscale circulations which can either favour or inhibit convection triggering (Findell and Eltahir, 2003a; Taylor et al., 2011; Rochetin et al., 2017).

In particular, irrigation can create strong spatial heterogeneities in SM. Observational studies have established that irrigation leads to a moister and cooler atmosphere near the surface (Bonfils and Lobell, 2007; McDermid et al., 2023), which is explained
50 by an increase in the latent heat flux and a decrease in the sensible heat flux in irrigated areas (Rappin et al., 2022; Boone et al., 2025). In the American Midwest, Nocco et al. (2019) showed that such effects could impact the regional climate and even mask the rise in temperature induced by global warming. Different regional responses of precipitation have also been observed, such as a decrease in irrigated areas (Alter et al., 2015) or an increase in downwind regions (DeAngelis et al., 2010).



To analyse the atmospheric processes involved, regional modelling studies have often been used to complement observational campaigns. The Great Plains irrigation experiment (GRAINEX, Rappin et al., 2021) measurements and simulations with the Weather Research and Forecasting (WRF) model revealed a lower ABL over irrigated areas and a reduction of existing mesoscale slope-induced circulations in the presence of irrigation (Rappin et al., 2022; Phillips et al., 2022). In the Ebro Valley (northern Spain), Meso-NH simulations over the area of the Land surface Interactions with the Atmosphere over the Iberian Semiarid Environment campaign (LIAISE Boone, 2019) were shown to be greatly improved by representing irrigation (Lunel et al., 2024a), and also highlighted a weakening of the regional sea-breeze regime due to irrigation (Lunel et al., 2024b). Lo and Famiglietti (2013) and Yang et al. (2017) studied the local and remote impacts of irrigation in California's Central Valley, showing a strengthening of the hydrological cycle, with moisture recycling at the river basin scale, whereas a similar study in Saudi Arabia identified a negative feedback loop with increases in precipitation located in a remote area (Lo et al., 2021).

These results, however, were obtained with very diverse representations of irrigation since not all models target the same objectives. For example, Lunel et al. (2024a) used an idealized representation that maintains SM at a certain level in irrigated areas. This type of modelling is suitable for short simulations over a limited domain but for Earth System Models (ESMs) running long simulations, water-conservative approaches are necessary. With this type of approach, Leng et al. (2017) identified contrasting responses in river discharge and water table depth depending on the irrigation methods represented.

At the global scale, the average impacts of simulated irrigation have been studied in land-atmosphere coupled simulations (Sacks et al., 2009; Puma and Cook, 2010; Pokhrel et al., 2012; Cook et al., 2015), with effects mostly visible in irrigation hotspots such as India, Eastern China and the United States of America. This type of study has also identified remote connections between irrigation in Asia and precipitation in East Africa (de Vrese et al., 2016), and between moisture-importing and moisture-exporting regions (Wei et al., 2013). However, only three CMIP6 models included a representation of irrigation, and Al-Yaari et al. (2022) showed that they better captured the trends of several climate variables over irrigated regions. Efforts are currently being pursued to better account for the impacts of irrigation in ESMs, as illustrated by the Irrigation Model Intercomparison Project (IRRMIP), which aims to compare the responses of various models to representations of irrigation (Yao et al., 2023, 2024).

ESMs are not expected to achieve the same level of precision as convection resolving models in their accounting for irrigation, but the extent to which their representation of irrigation can impact the simulated climate in irrigated regions is still not well constrained. In this context, this study aims to understand which regional impacts of irrigation on surface-atmosphere couplings and the water cycle can be represented by a climate model. It leverages a new limited area model configuration developed for the Institut Pierre-Simon Laplace climate model (IPSL-CM) to perform regional simulations with the land surface and atmospheric components of the global model, ORCHIDEE (Krinner et al., 2005; Cheruy et al., 2020) and ICOLMDZ (Dubos et al., 2015; Hourdin et al., 2020). This configuration allows for insight on the parameterizations of the global model while running with a higher resolution (25 km) and lower computational costs than in global applications.

This work is based on two regional simulations (with and without irrigation) over the Iberian Peninsula between 2010 and 2022, analysed on yearly and seasonal scales. Section 2 provides a detailed description of the modelling design and reference products used to evaluate the simulations. Section 3 presents an evaluation of irrigation volumes, river discharge, precipitation



and ET, and a comparison of the two simulations to isolate the effects of irrigation and analyse continental moisture recycling.

90 Finally, Section 4 presents the conclusions, as well as a discussion of the limitations and future developments of this work.

2 Methods

2.1 ICOLMDZOR limited area model

This study uses the atmosphere and land surface components of the IPSL-CM, which has been a regular participant in CMIP, including CMIP6 (Boucher et al., 2020). The simulations are run with prescribed sea surface temperature and sea ice content

95 from the Atmospheric Model Intercomparison Project (AMIP) dataset.

2.1.1 ICOLMDZ atmospheric model

The atmospheric component of the model is the association of the dynamical core DYNAMICO (Dubos et al., 2015), which uses an icosahedral grid, and the LMDZ6A physics version NPv6.2 used for CMIP6, with 79 vertical levels (Hourdin et al., 2020). The physics of the model are run every 15 mn and include the following parameterizations:

- 100 – a surface layer description based on Louis (1979) and King et al. (2001);
- an eddy-diffusivity mass flux (EDMF) scheme of boundary layer vertical transfer composed of a turbulent diffusion scheme based on Yamada (1983) with recent improvements described in Vignon et al. (2018), and a thermal plume model for shallow convection (Rio and Hourdin, 2008; Hourdin et al., 2019);
- a mass-flux scheme for deep convection based on Emanuel’s scheme (Emanuel, 1991; Grandpeix et al., 2004; Rio et al., 105 2013), with stochastic triggering (Rochetin et al., 2014a, b);
- a parameterization of the cold pools created below cumulonimbus clouds by reevaporation of convective rainfall (Grandpeix and Lafore, 2010; Grandpeix et al., 2010);
- a large scale condensation scheme based on a statistical distribution of the subgrid total water content, from which the cloud fraction and water contents are derived (Madeleine et al., 2020);
- 110 – the radiative transfer model RRTM (Mlawer et al., 1997).

Regional simulations are run using a limited area model (LAM) configuration, which was first used and described in Raillard et al. (2024). Lateral boundary conditions for the LAM are read at each time step of the dynamics, and are taken from ERA5 reanalysis hourly values at 0.25° resolution (Hersbach et al., 2020). The LAM domain comprises 3 zones: a raw forcing zone that contains values directly given by the forcing, a transition zone where the model is nudged towards the forcing with 115 decreasing strength, and a free zone at the centre of the domain where there is no direct influence of the lateral forcing. The outputs of the model are natively on a hexagonal grid but are interpolated to a more traditional longitude-latitude grid of similar resolution, to simplify posttreatment and comparisons to evaluation products.



2.1.2 ORCHIDEE land surface model

Water and energy budgets

120 The ICOLMDZ LAM is coupled to the ORCHIDEE v2.2 land surface model (LSM) (Krinner et al., 2005; Cheruy et al., 2020). The spatial grid of the LSM is the same as that of the LAM and the timestep is dictated by that of the atmospheric physics (15 mn). ORCHIDEE represents a 2 m soil column discretized along 11 vertical layers of increasing thickness. It computes the coupled water and energy budgets at the surface by simulating, among other processes, latent and sensible heat fluxes, surface runoff and water infiltration in the soil column, with a free drainage condition at the bottom. Each grid cell is assigned
125 the dominant United States Department of Agriculture (USDA) soil texture according to the 5 arcmin resolution map from Reynolds et al. (2000). Vegetation is described using 15 plant functional types (PFTs) from a 0.1° resolution input map based on the Land Use Harmonization 2 (LUHv2) dataset (Hurt et al., 2020; Lurton et al., 2020). In each grid cell, PFTs are clustered into 3 soil tiles, for bare soil, forests, and low vegetation (including C3 and C4 crops). The model computes a separate water budget for each soil tile but only one energy budget per grid cell, using a composite approach with aggregated parameters
130 (roughness length, albedo, aridity factor) to compute surface temperature and turbulent fluxes.

Routing scheme

River discharge is simulated using a routing scheme based on the one described in Ngo-Duc et al. (2007). This scheme solves horizontal water transfers on the digital elevation model (DEM) grid, here upscaled at a 2 km resolution from the MERIT DEM (Yamazaki et al., 2019). Each DEM grid cell contains three linear reservoirs that provide overland flow, groundwater
135 flow and river flow. For each reservoir, the characteristic residence time of water in a grid cell depends on a fixed transfer coefficient and on the slope provided by the DEM. The surface runoff and drainage computed for each ORCHIDEE soil column are interpolated to the routing grid to feed the overland and groundwater reservoirs, respectively. Water from all three reservoirs flows into the river reservoir of the downstream grid cell. In this scheme, river reservoirs constitute the only means of grid-to-grid horizontal water transfer.

140 Irrigation

Irrigation is modelled using the scheme extensively described in Arboleda-Obando et al. (2024), which is based on a water-conservative supply-and-demand approach. It computes a moisture deficit by comparing SM in the upper layers of the ORCHIDEE soil column (64 cm, corresponding to the root zone) to a target SM described as a fraction of the SM at field capacity. In the default version of the global model, this target is set to 90 % of the SM at field capacity, but it reflects a wide variety of
145 irrigation practices, including flooding in rice paddies. In the Iberian Peninsula, the irrigation methods are less water-intensive, and after calibrating the routing and irrigation schemes (not shown), the target value was adjusted to 60 % of the SM at field capacity. To avoid computing irrigation requirements on grid cells without plants, the SM deficit is set to zero if the leaf area index (LAI) is below a given threshold $LAI_{min} = 0.1$.

At each time step, the SM deficit is weighted by the irrigated fraction of each ORCHIDEE grid cell, based on the historical
150 irrigation dataset (HID, Siebert and Döll, 2010) at 5 arcmin resolution, to define the irrigation requirement. This demand is then compared with the available water in the three reservoirs of the routing module. Only 90 % of the volume can be



withdrawn from each reservoir to maintain a minimum environmental flow. Water is withdrawn preferentially from either surface water (overland and rivers) or groundwater depending on the nature of irrigation equipment, defined by the map of Siebert et al. (2010). It must be noted that although the original irrigation scheme from Arboleda-Obando et al. (2024) included the possibility to withdraw water from neighbouring grid cells to represent adduction systems, this option is not yet compatible with the new version of the routing scheme and was not used in this study. As a final step, the amount of water withdrawn from the reservoirs is added at the top of the ORCHIDEE soil column at the next time step for infiltration.

2.2 Simulation setup

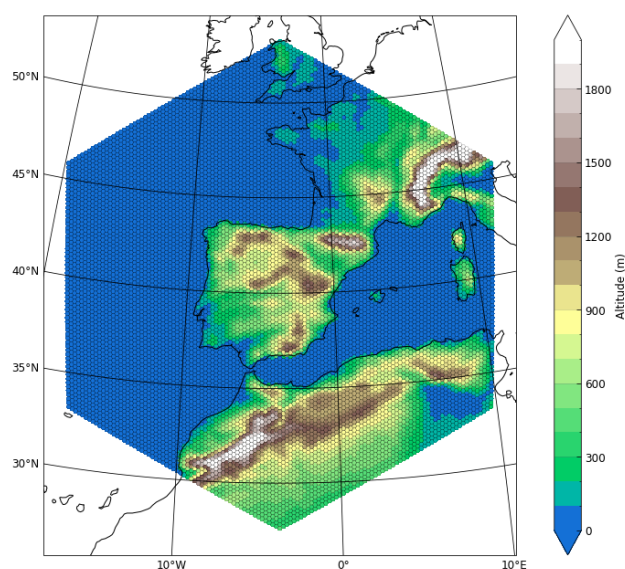


Figure 1. Altitude (m) over the simulation domain on the native hexagonal grid.

The Iberian Peninsula was chosen as the study region since it is a hotspot for irrigation in Europe, particularly in the Ebro Valley (northern Spain). In addition, it is clearly bounded by the Atlantic Ocean, the Mediterranean Sea, and the Pyrenees mountain range in the north, which ensures that all watersheds are fully included in the simulation domain, making the regional study of the continental water cycle rather straightforward. Moreover, although it was not identified by Koster et al. (2004) as a region of strong coupling, probably owing to its small size relative to the resolution of the model used and to other identified hotspots, its semiarid climate should make it very sensitive to the influence of land surface-atmosphere coupling processes. Therefore, modifications of the SM heterogeneity patterns induced by irrigation are expected to have a clear influence on the local and regional climates.

To study this region, the LAM simulation domain is a hexagon (centred at 40.4° N, -3.7° E) with a radius of 1500 km (Fig. 1). The radius is composed of 60 grid cells, so the diameter of each cell is 25 km. The simulations are run for 13 years from 2010 to 2022, which enables capturing some interannual variability of the current climate, making the averages less sensitive



170 to anomalies or biases from any single year or extreme event. Before this 13 year simulation, 3 years were run as a warm-up to allow for the hydrological and vegetation variables to reach a satisfactory equilibrium. Two simulations are run with the same setup except for the inclusion of irrigation. They are referred to as *irr* (with irrigation activated in ORCHIDEE) and *no_irr* (without irrigation). Considering the focus on land-atmosphere coupling, the analysis is restricted to the Iberian Peninsula, thus excluding ocean grid cells and the land grid cells north of the Pyrenees, which flow to France. To prevent mismatches between
175 the simulations and the evaluation datasets because of different coastlines, the analysis is further reduced to grid cells where the continental fraction is greater than 95 % .

2.3 Evaluation datasets

Table 1. Gridded datasets used for evaluation.

Dataset	Variables used	Unit	Resolution	Available period	References
GPCC	Precipitation	mm d ⁻¹	0.25°	2010-2019	Schneider et al. (2020)
GLEAMv4.1a	ET	mm d ⁻¹	0.25°	2010-2022	Martens et al. (2017); Miralles et al. (2025)
Ebro irrigation estimate	Irrigation	mm d ⁻¹	1 km	01/2016-07/2020	Dari et al. (2023)

The simulations are evaluated against the monthly mean values of the reference gridded products listed in Table 1. Precipitation data from the Global Precipitation Climatology Centre (GPCC) Full Data Monthly Product Version 2020 (Schneider et al.,
180 2020) is used. This reanalysis product provides precipitation data until 2019 over land on a 0.25° x 0.25° grid using in situ rain gauges. For ET, the Global Land Evaporation Amsterdam Model (GLEAM) dataset is used, in its fourth version (Miralles et al., 2025). This product computes ET using a large set of input variables obtained from reanalyses as well as in situ and satellite observations. Monthly values at 0.25° resolution are used, initially given in mm month⁻¹ but converted to mm d⁻¹. GLEAM4 is available until 2022 but since precipitation and ET are evaluated jointly, it is only used over the availability period
185 of GPCC data (2010-2019). Simulated irrigation is evaluated in the Ebro Valley region using a high resolution remote sensing product from the European Space Agency (ESA) Irrigation+ project (Dari et al., 2023). This product estimates irrigation with a soil moisture based approach using satellite measurements from Sentinel-1, and provides data for three intensely irrigated areas: the Ebro Basin in Spain, the Po Valley in Italy and the Murray-Darling Basin in Australia. From 2016 to 2020 in the Ebro Basin, the median values of the RMSE, Pearson correlation coefficient *r* and bias are 12.4 mm over 14 days, 0.66, and
190 -4.62 mm over 14 days, respectively. Weekly values are aggregated to a monthly average in mm d⁻¹. The simulated river discharge is evaluated against monthly observation data from discharge stations of the Global Runoff Data Center (GRDC, <https://grdc.bafg.de>, Fekete, 2003). Stations were positioned on the MERIT DEM grid with tools presented in Polcher et al. (2023), which use the GPS position of the stations as well as the upstream catchment area to find the most appropriate grid cell for comparison with the observations. The 18 selected stations with available data over the simulation period and an adequate



195 position on the DEM grid are described in Table 2 and shown in Fig. 2. Most stations have available data from January 2010 to September 2017, and river discharge was therefore evaluated using the first eight years of simulation (2010-2017).

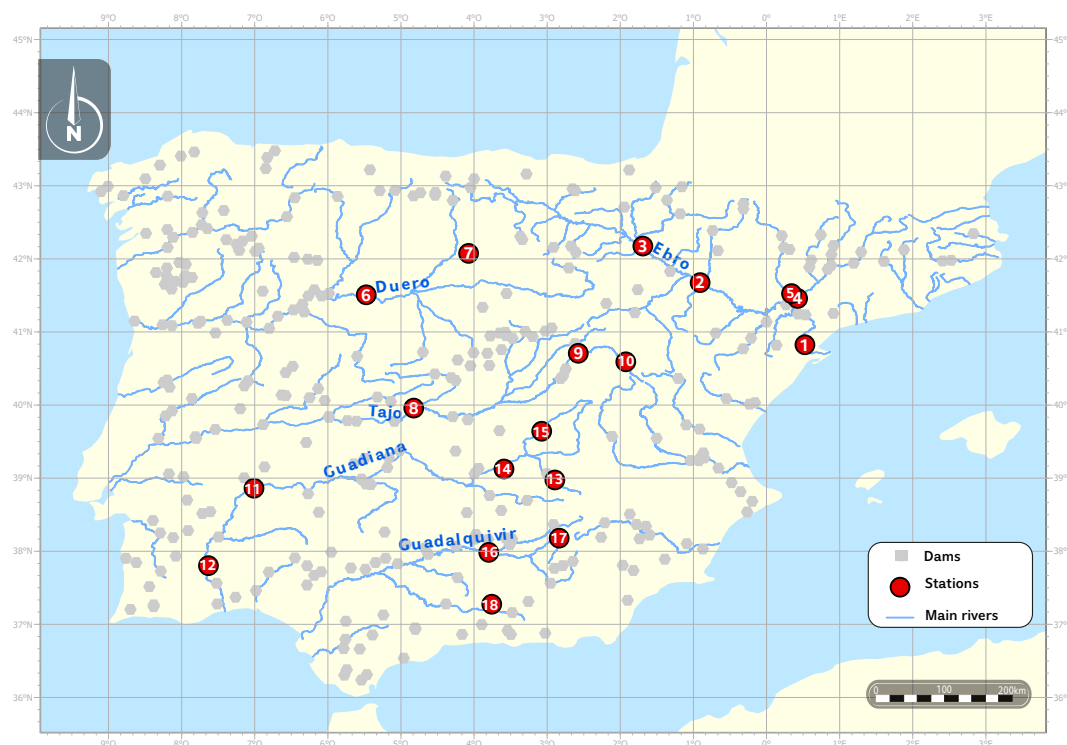


Figure 2. Stations used for river discharge evaluation, river dams from Aquastat Geo-reference Database on Dams, and main rivers of the study area from the CCM2.1 dataset (Vogt et al., 2007), showing only rivers longer than 50 km for readability.

2.4 Statistical significance

To assess the influence of irrigation on the model, the two simulations (*irr* and *no_irr*) are compared and a statistical significance test is used to filter out differences that may be the result of natural variability only. For the maps of changes induced by irrigation in Sect. 3.4, a Student t-test is used to assess for each grid cell whether the mean difference between the two simulations (*irr* - *no_irr*) significantly differs from 0, with a p-value of 0.05 as the limit to reject the null hypothesis. Grid cells with nonsignificant changes are partly hidden with hatches.



Table 2. Characteristics of river discharge stations used for evaluation. Stations marked with * are the largest of the five major basins of the Peninsula, and are shown in Fig. 5

Station	Altitude (m)	River	Area (km ²)	Mean discharge (m ³ /s)	Coverage (2010-2017, %)
*1 (Tortosa)	25	Ebro	84230	287.61	96.9
2 (Zaragoza)	189	Ebro	40434	210.89	96.9
3 (Castejon)	265	Ebro	25194	201.34	96.9
4 (Seros)	85	Segre	12782	52.75	96.9
5 (Fraga)	100	Cinca	9612	49.69	93.8
*6 (Tore)	637	Douro	41808	109.18	96.9
7 (Peral De Arlanza)	766	Arlanza	2413	16.44	96.9
*8 (Talavera)	366	Tagus	33849	46.77	34.4
9 (Trillo)	727	Tagus	3253	12.70	96.9
10 (Peralejos)	1143	Tagus	410	3.87	96.9
*11 (Azud de Badajoz)	166	Guadiana	48530	81.83	83.3
12 (Pulo do Lobo)	28	Guadiana	61884	25.23	58.3
13 (La Cubeta)	758	Guadiana	856	3.37	92.7
14 (Villarubia)	628	Guadiana	10319	0.82	66.7
15 (Quintanar)	694	Giguela	995	0.71	55.2
*16 (Mengibar)	240	Guadalquivir	16166	30.25	75.0
17 (Arroyo Maria)	538	Guadalquivir	583	6.19	86.5
18 (Pinos Puente)	561	Frailes	357	1.00	87.5

3 Results

3.1 Simulated irrigation

205 The computed irrigation demand (Fig. 3c) is highly dependent on the irrigated fraction (Fig. 3a) and much greater than the applied irrigation (Fig. 3d). This shows that irrigation is often constrained by water availability, with clear regional differences. Indeed, irrigation is much greater in the northern regions (Ebro and Douro river basins) than in southern regions (Guadiana and Guadalquivir basins) even though these regions have similar levels of irrigation demand (Fig. 3c, d). As shown in Fig. 3b, southern regions (Guadalquivir Basin, upper Guadiana Basin) are more dependent on groundwater equipment for irrigation

210 water withdrawals than the Ebro Basin, where withdrawals are taken mainly from surface water (overland and river reservoirs in the model). Considering that the groundwater reservoir is much more depleted in the presence of irrigation than the river reservoir is (Fig. 3e, f), it is not surprising that the irrigation requirement cannot be met in these regions as much as it is in the north. This depletion can be explained by the fact that the groundwater reservoir can only be filled with drainage in the

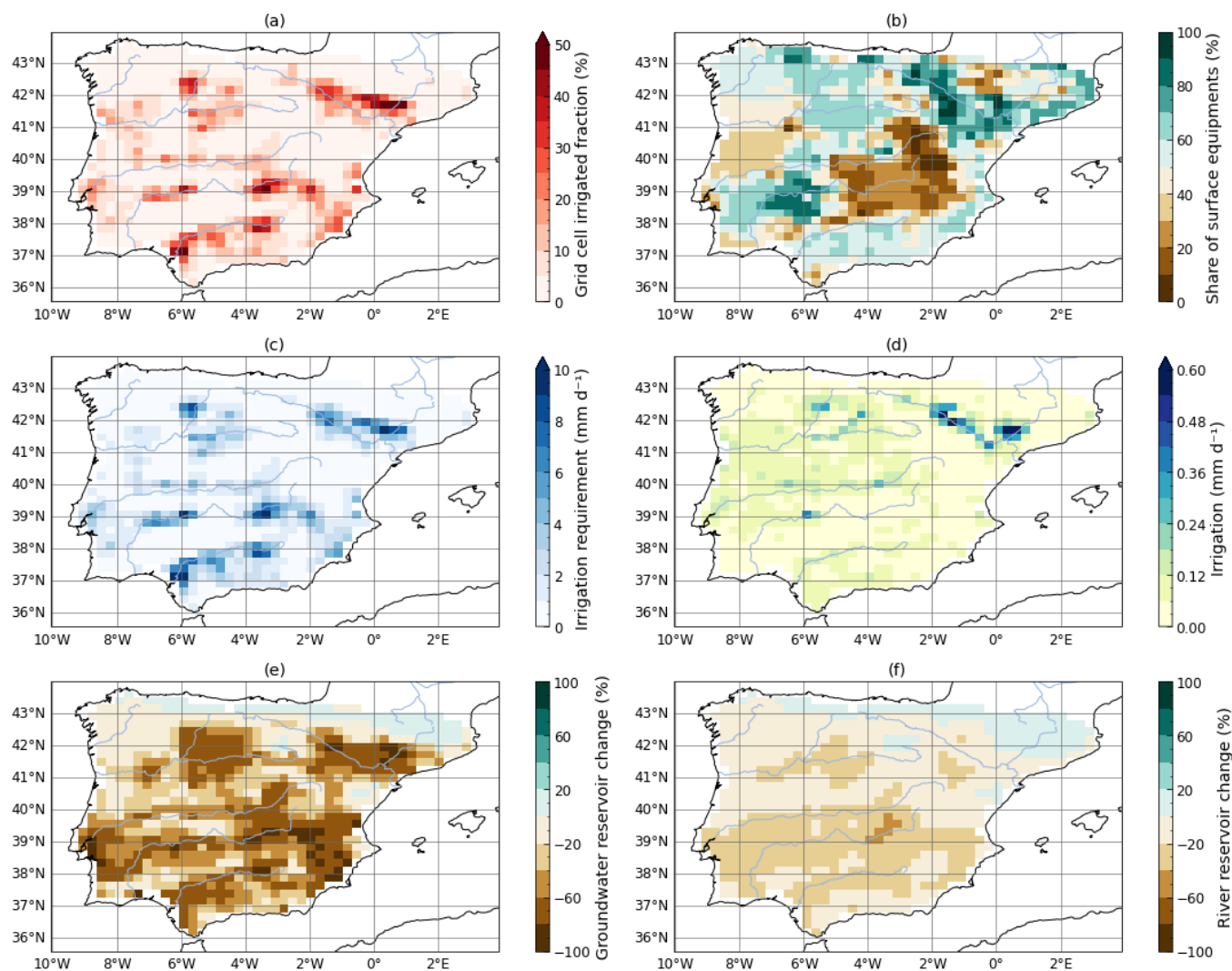


Figure 3. Simulated irrigation and its drivers. Input maps of (a) grid cell irrigated fraction (% , derived from Hurtt et al., 2020) and (b) the share of irrigation equipment for surface withdrawals, as opposed to groundwater withdrawals (% , derived from Siebert et al., 2010). Annual means (2010-2022) of (c) simulated irrigation requirement (mm d⁻¹), (d) irrigation (mm d⁻¹), and relative changes ($irr - no_irr$, %) in water volumes in (e) groundwater and (f) river reservoirs.

grid cell, whereas the river reservoir can be fed from upstream grid cells. It is also important to note that ORCHIDEE does not
215 model deep groundwater storage, which is an important source of water for irrigation in southeastern Spain (Custodio et al., 2016).

In the Ebro Basin, simulated irrigation is evaluated using the irrigation remote sensing product from Dari et al. (2023) with good overall performance, particularly in summer (Fig. 4a). In winter, the model simulates almost no irrigation since it requires

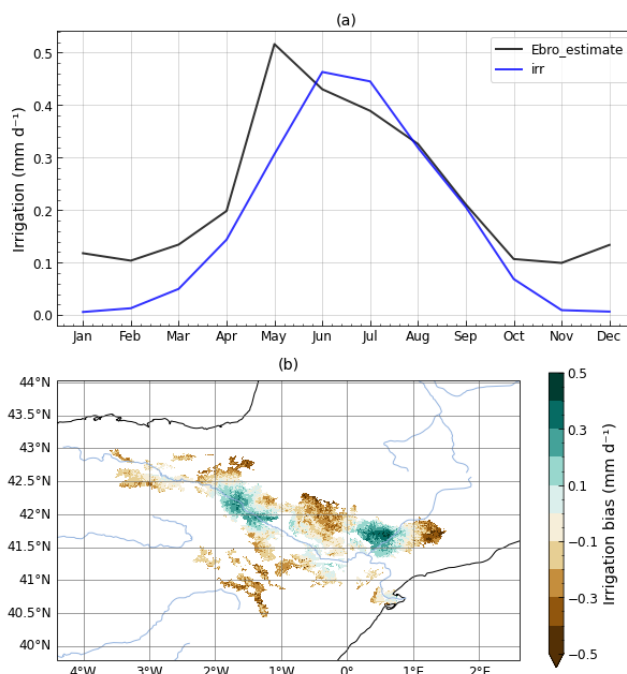


Figure 4. Evaluation of simulated irrigation from January 2016 to July 2020 over the Ebro Valley. (a) Mean seasonal cycle of irrigation for the *irr* simulation and the remote sensing product (*Ebro_estimate*, mm d^{-1}), and (b) mean bias compared with the product (mm d^{-1}). The simulation outputs are interpolated on the grid of the remote sensing product.

a minimum LAI to be activated, whereas the product shows irrigation all year long, which can be explained by the presence of winter crops not represented in the model. A delay of the summer peak in the model compared with the product is noticeable, but the model might not be very far from actual irrigation since this product was found to be slightly ahead of actual irrigation based on benchmark volumes in some districts of the Ebro Valley (Fig. 5 in Dari et al., 2023). Spatially, the remote sensing product shows greater irrigation on the hillslopes than in the thalwegs, whereas the model simulates the opposite, with more intense irrigation next to the large rivers (Ebro, Segre, Cinca). The resulting bias pattern (Fig. 4b) can be explained by the fact that in the model, water is mainly withdrawn from the river reservoir in this region, which is much greater in grid cells holding a large river than in upper areas of the valley. In reality, infrastructures such as the Canal d’Urgell in the Segre basin (Farran, 2024), enable gravity irrigation of hillslopes by diverting water from large rivers to neighbouring croplands. Including a representation of water adduction in the irrigation scheme by enabling withdrawal from adjacent grid cells could be a way to improve this bias. Overall, the spatial biases of the simulated irrigation offset each other relatively well. Averaged over the subdomain where the satellite product provides values, the simulated irrigation is 0.20 mm d^{-1} while the product estimates it at 0.23 mm d^{-1} .



3.2 Impacts of irrigation on river discharge

Figure 5 shows the average seasonal cycle of river discharge for the five largest rivers of the Peninsula (Ebro, Douro, Tagus, Guadiana, and Guadalquivir), for the two simulations and the GRDC observation data. The station with the greatest river discharge was selected for each river, to reflect integrated impacts of irrigation over the basin. A similar figure with all eighteen stations is presented in the appendix (Fig. A2). In most cases, the model shows a slight delay and a large overestimation of river discharge compared with observations, particularly in winter and spring. These errors can be related to the precipitation biases of the simulations, described in the next section, and to the lack of river dams in the model, which have a strong impact on actual discharge, given their high density in the Iberian Peninsula (Fig. 2, Sabater et al., 2022; Morán-Tejeda et al., 2012; Lobera et al., 2015). In particular, the model overestimates the winter and spring discharge, a period when water is stored in dam reservoirs, which reduces the actual river flow. The presence of dams also leads to unnatural seasonal cycles in the observations if river discharge is artificially increased in summer by the release of stored water (Fig. 5e).

The simulation of irrigation used cannot improve either of these aspects since it does not include a specific reservoir to store water. Its impact becomes noticeable in spring, with water withdrawals resulting in lower discharge during summer and autumn, generally leading to a much better match with observations (Fig. 5). As shown in Table 3, for all fifteen stations where the mean bias is positive in the *no_irr* simulation, this bias is reduced in the presence of irrigation (in three cases it becomes negative but the absolute value is reduced). However, for the three stations where the *no_irr* bias is negative (n°10, 13, 17), it is worsened in the *irr* simulation. On average, the *irr* simulation exhibits clear improvements of the mean bias (-41.8 %) and root mean square error (RMSE, -7.12 %). The Pearson correlation coefficient is 0.56 on average in *no_irr* and is slightly improved (+0.02), with mostly small changes except for stations 6 and 8 (+0.09 and +0.08). Improvements are also observed for Nash-Sutcliffe efficiency (NSE, +0.67) and Kling-Gupta efficiency (KGE, +0.2), mostly as a consequence of improvements in the mean bias. However, only eight out of eighteen stations have a positive value of NSE and KGE values in the *no_irr* simulation (not shown), limiting the relevance of this average increase. In particular, the average NSE value is strongly influenced by a few stations (n°5, 8, 15) with initial NSE values below -10.

Overall, the performance is clearly improved for 12 stations but partly degraded for 6 stations, although three of them (n°10, 13, 17) have a very small average discharge. This may explain why small changes in the model can lead to large changes in performance and limits their relevance compared with larger stations. If only stations with an average annual discharge greater than $10 \text{ m}^3 \text{ s}^{-1}$ are considered, irrigation improves performance in nine out of twelve cases, and degrades it for three stations. One station (n°9) exhibits an unexpected increase in the spring discharge peak which originates mostly from a single year (2011, see Fig. A1) and worsens an already-existing 250 % bias in this season. The other two (n°4 and 5) are close to the Pyrenees Mountains and present very strong biases in both simulations (300 % overestimation in spring, unexpected double peak in March and June, Fig. A2). These discrepancies are likely related to biases in precipitation (discussed hereafter) and were not positively impacted by irrigation, apart from the mean bias.



Table 3. Station mean discharge (*obs*, $\text{m}^3 \text{s}^{-1}$), discharge bias (for the *no_irr* and *irr* simulations, in %), and change in evaluated metrics (*irr* - *no_irr*) for the RMSE (relative change in %), Pearson correlation coefficient *r*, Nash-Sutcliffe efficiency and Kling-Gupta efficiency. Model performance improvements when using irrigation are shown in bold. Stations marked with * are the largest of the five major basins of the Peninsula, and are shown in Fig. 5.

Station	Mean discharge (<i>obs</i> , $\text{m}^3 \text{s}^{-1}$)	Bias (<i>no_irr</i> , %)	Bias (<i>irr</i> , %)	RMSE change (<i>irr</i> - <i>no_irr</i> , %)	<i>r</i> change (<i>irr</i> - <i>no_irr</i>)	NSE change (<i>irr</i> - <i>no_irr</i>)	KGE change (<i>irr</i> - <i>no_irr</i>)
*1 (Tortosa)	287.61	126.3	103.4	-7.88	0.03	0.56	0.13
2 (Zaragoza)	210.89	27.6	11.5	-13.10	0.01	0.06	0.10
3 (Castejon)	201.34	30.7	21.4	-1.45	0.01	0.01	0.03
4 (Seros)	52.75	240.3	227.7	0.81	-0.02	-0.54	-0.09
5 (Fraga)	49.69	193.2	179.8	1.81	-0.01	-1.78	-0.22
*6 (Tore)	109.18	36.9	-0.2	-16.24	0.09	0.21	0.25
7 (Peral De Arlanza)	16.44	40.7	35.2	-3.12	0.01	0.04	0.04
*8 (Talavera)	46.77	152.4	95.8	-10.84	0.08	2.29	0.16
9 (Trillo)	12.70	60.8	59.7	0.76	0.03	-0.15	-0.05
10 (Peralejos)	3.87	-34.6	-38	1.82	0.01	-0.03	-0.01
*11 (Azud de Badajoz)	81.83	90.5	34.3	-14.26	0.05	0.24	0.51
12 (Pulo do Lobo)	25.23	287.3	162.0	-18.53	0.03	1.48	1.17
13 (La Cubeta)	3.37	-10.7	-36.2	5.82	-0.01	-0.12	-0.12
14 (Villarubia)	0.82	152.4	61.0	-3.53	-0.03	0.29	0.53
15 (Quintanar)	0.71	312.7	149.3	-17.89	0.00	9.31	0.98
*16 (Mengibar)	30.25	19.4	-16.9	-4.52	0.01	0.46	0.09
17 (Arroyo Maria)	6.19	-35.4	-47.5	8.44	-0.04	-0.28	-0.10
18 (Pinos Puente)	1.00	27.0	-3.0	-5.59	0.03	0.06	0.12
Mean	63.37	95.4	55.5	-7.12	0.02	0.67	0.20

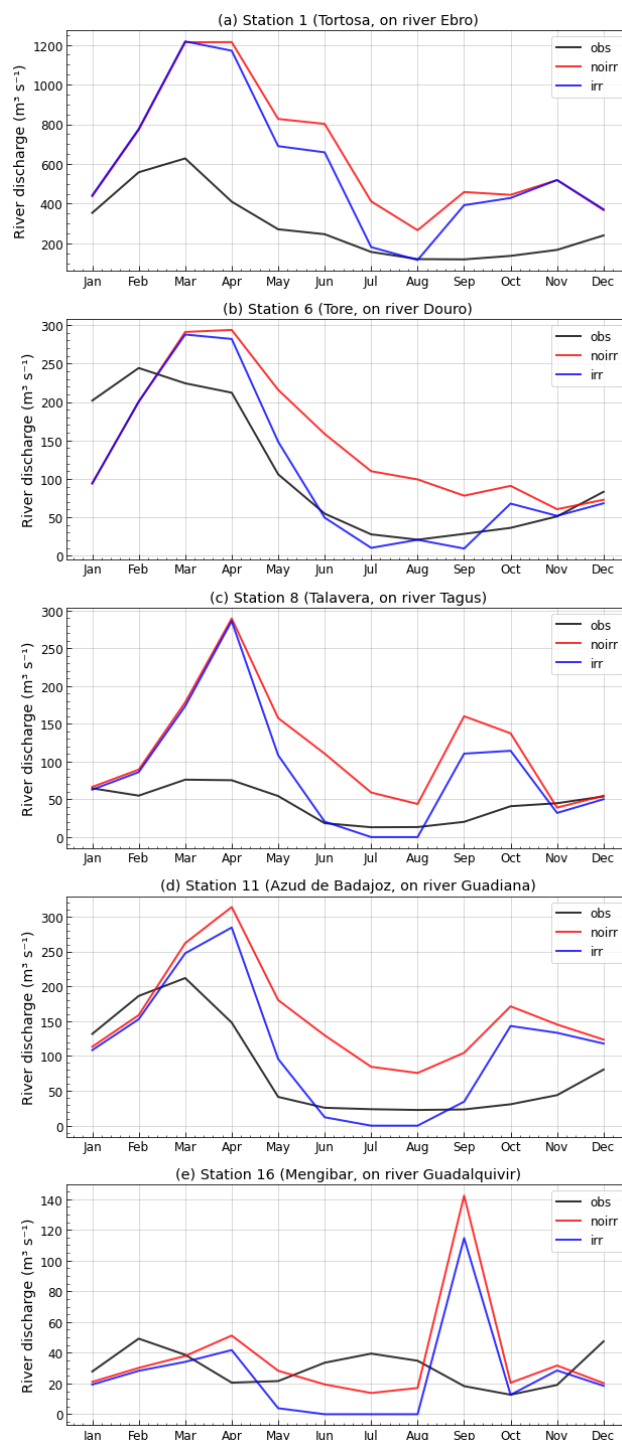


Figure 5. Impacts of irrigation on river discharge. Mean seasonal cycle of river discharge ($\text{m}^3 \text{s}^{-1}$) in observations (black) and the *no_irr* (red) and *irr* (blue) simulations at five stations: (a) Tortosa (Ebro), (b) Tore (Douro), (c) Talavera (Tagus), (d) Azud de Badajoz (Guadiana), and (e) Mengibar (Guadalquivir). A mask is applied to the simulations to filter out months without corresponding observation data.



3.3 Evaluation of precipitation and ET and influence of irrigation

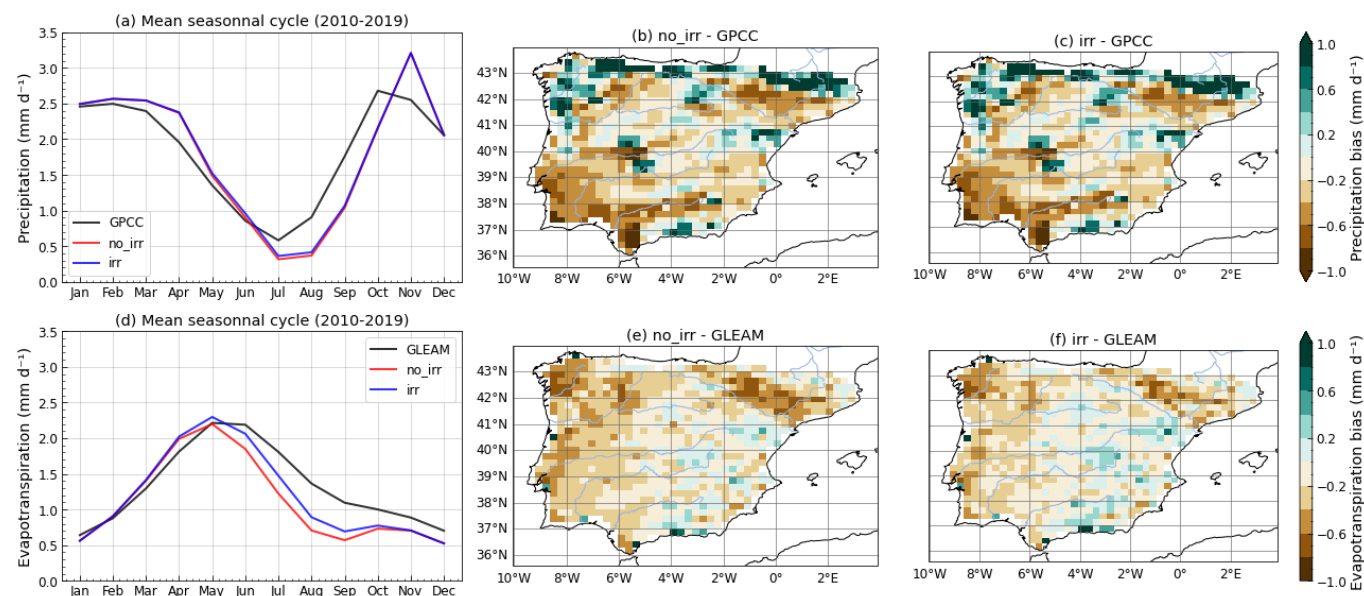


Figure 6. Evaluation of simulated precipitation (P) and evapotranspiration (ET) over the Iberian Peninsula continental subdomain, from 2010 to 2019. (a) Mean seasonal cycle of P (mm d^{-1}) for the two simulations and GPCC product, annual mean P bias of the (b) *no_irr* and (c) *irr* simulations relative to the GPCC product (mm d^{-1}). (d) Mean seasonal cycle of ET (mm d^{-1}) for the two simulations and GLEAM4 product, annual mean ET bias of the (e) *no_irr* and (f) *irr* simulations relative to the GLEAM4 product (mm d^{-1}).

265 The simulated precipitation and ET are evaluated from 2010 to 2019 using the GPCC and GLEAM4 products, respectively (Fig. 6). On average over the domain, the two simulations present very similar seasonal cycles of precipitation. The model is in good agreement with GPCC until June (Fig. 6a), but presents a strong underestimation of precipitation in summer, followed by a delayed and overestimated peak in autumn, which likely contributes to the biases of river discharge winter peaks visible in Fig. 5. This seasonal cycle is largely representative of the whole peninsula, although some spatial disparities persist. The two simulations exhibit very similar spatial patterns of annual mean precipitation, with a strong overestimation in elevated areas (Fig. 6b,c), which is a known bias of climate models (Arjdal et al., 2024; Adhikari et al., 2024). This is partly compensated by smaller underestimates of precipitation over large neighbouring areas, as seen in the Ebro Valley.

Both simulations match the GLEAM4 ET product well from January to May but underestimate ET for the rest of the year, particularly in summer (Fig. 6d). As expected, ET increases when irrigation is accounted for, particularly from May to September, which is the period where vegetation is the most developed and irrigation is the greatest. This partially alleviates the dry bias, but ET remains underestimated, even in the *irr* simulation. No similar patterns of biases between ET and incoming radiative fluxes were identified, and the remaining ET bias can be related to the underestimation of precipitation in the southwestern part of the Peninsula and in plains, such as the northern Ebro Valley (Fig. 6b, e). Along large rivers, the ET underestimation al-



most disappears in the *irr* simulation (Fig. 6f). The increase in soil moisture due to irrigation directly translates into an increase
280 in ET, corroborating the hypothesis that the region lies within the transition regime described by Budyko (1956). In contrast,
the ET bias remains significant in lightly irrigated grid cells such as hillslopes, which is consistent with the limits of simulated
irrigation described in Section 3.1 (Fig. 4).

3.4 Atmospheric impacts of irrigation in summer

Here, the impacts of irrigation on atmospheric variables are studied in summer (JJA) since it is the season with the highest levels
285 of simulated irrigation, with seasonal mean values of up to 1.5 mm d^{-1} in the most intensely irrigated grid cells (Fig. 7a). In
the presence of irrigation, the simulated latent heat flux (LE) increases across the entire Iberian Peninsula, by up to 50 W m^{-2}
in the Ebro Valley. As expected from the surface energy partitioning, this is compensated by a decrease in the sensible heat flux
(H), which is almost equivalent in irrigated areas and leads to large increases in the evaporative fraction ($EF = \frac{LE}{LE+H}$) shown
in Fig. 7b. When the sensible heat flux decreases, less energy is transmitted from the surface to the air, leading to a decrease
290 in the 2 m air temperature which spatially matches the increase in EF . The order of magnitude remains low over most of the
Peninsula, with the most important changes reaching -0.35 K in the Ebro Valley (Fig. 7c). The decreases in sensible heat flux
and temperature also lead to a more stable boundary layer over most of the peninsula, but mostly in intensely irrigated areas
where it is lowered by 100 m (Fig. 7d). Moreover, the presence of irrigation results in a moister lower atmosphere, with an
average specific humidity over the Peninsula increasing by $2.8 \cdot 10^{-4} \text{ kg kg}^{-1}$ in summer (+3.4 %) and maximal local increases
295 in the Ebro Valley of $1 \cdot 10^{-3} \text{ kg kg}^{-1}$ (+10 %). Since air temperature changes in the atmospheric column are rather small, the
lowering of the lifting condensation level (LCL) reflects this atmospheric moistening very well. It is most marked in the Ebro
Valley, where the LCL is lowered by 250 m (-13 %) in the most intensely irrigated grid cells, and remains significant even in
areas where irrigation is low (Fig. 7e).

The lowering of the ABL and LCL theoretically favour opposite effects on precipitation. On the one hand, a lower and
300 more stable ABL inhibits vertical mixing and convection, reducing the likelihood of cloud formation and deep convection
initiation. On the other hand, if the LCL is lower, air parcels do not need to be lifted as high to condense, which increases
the likelihood of cloud formation. Over the most intensely irrigated areas, ABL stabilization seems to dominate and inhibit
convective development since no significant change in precipitation is observed. However, mountainous areas surrounding the
Ebro Valley show significant increases in precipitation (Fig. 7f). This can be understood because ABL stabilization remains
305 weak in these zones whereas humidity can still be increased if moisture is advected (Fig. 7d, e). In particular, the dominant
wind patterns in the Ebro Valley (Fig. 7a) indicate that the additional atmospheric moisture from irrigated areas is driven
towards the valley slopes, which is consistent with the increases in moisture convergence (Fig. 7h) and precipitation over
the Pyrenees. The competing interactions of ABL stabilization and atmospheric moistening are reflected by the increases in
convective available potential energy (CAPE) which are most important in elevated areas around the valley (Fig. 7g), where
310 increases in precipitation are significant.

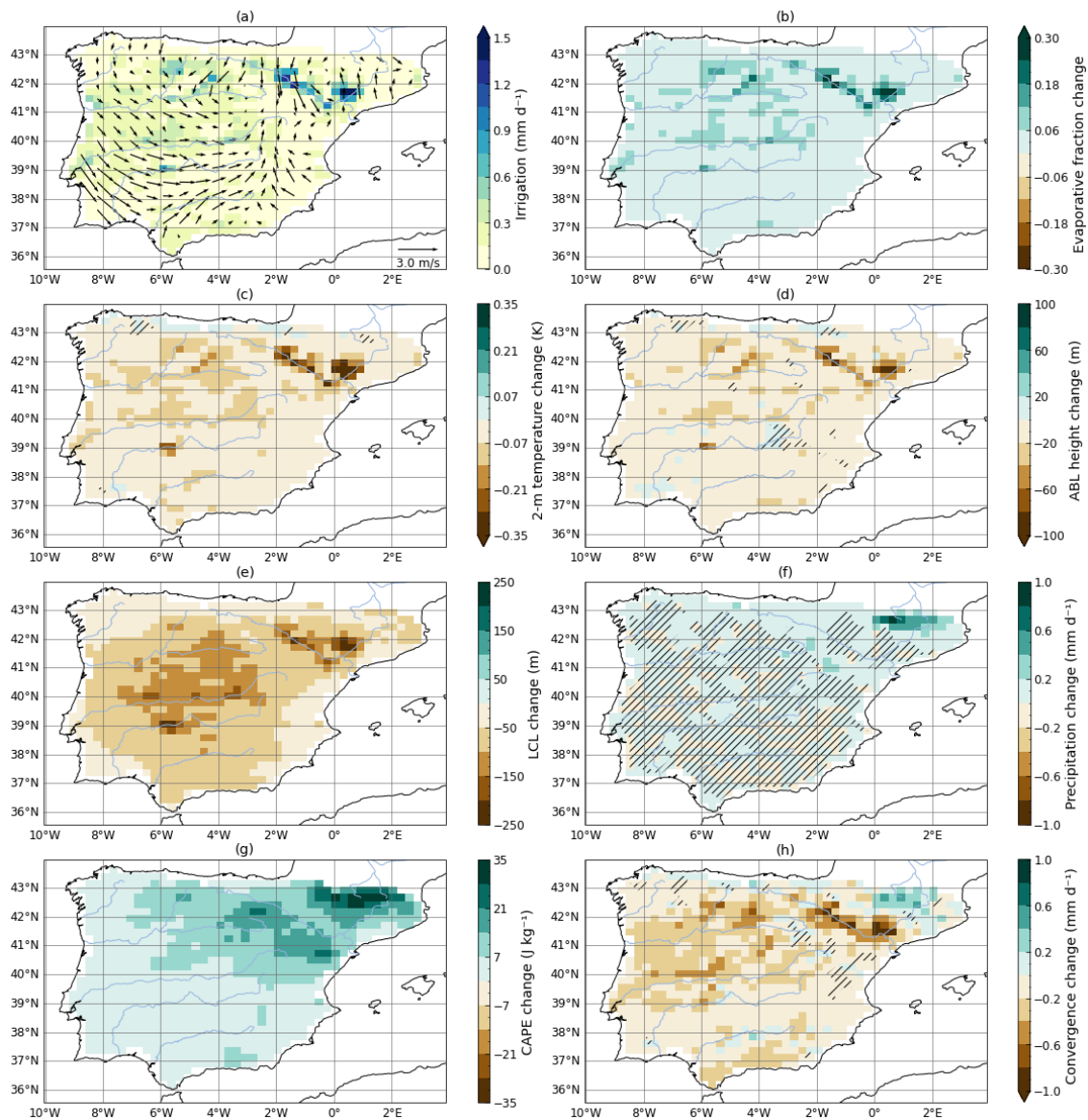


Figure 7. Summer irrigation and its impacts (JJA, 2010-2022). (a) Irrigation (mm d⁻¹) and 10 m wind (*irr* simulation). Mean changes in the presence of irrigation (*irr* - *no_irr*): (b) evaporative fraction, (c) 2 m temperature (K), (d) atmospheric boundary layer height (m), (e) lifting condensation level (m), (f) precipitation (mm d⁻¹), (g) convective available potential energy (J kg⁻¹), (h) moisture convergence (mm d⁻¹). Hatching indicates areas where the change is not statistically significant.



3.5 Atmospheric moisture recycling over the Iberian Peninsula

On average over the continental domain, the monthly change in ET in the presence of irrigation is well correlated with the amount of water added by irrigation and even exceeds it, particularly in summer months (the orange JJA data points in Fig. 8a are all on or above the 1:1 line). In the simulation, ET is constrained by available water, and almost all the water added by irrigation is evaporated or transpired, meaning that this additional increase in ET comes from an additional input of water into the soil. This is explained by a systematic increase in precipitation over the domain (all the data points are on or above the x-axis on Fig. 8b). This increase is also roughly proportional to the amount of applied irrigation, although the correlation is weaker than that for the increase in ET, and its values remain lower than the amount of water added by irrigation. Therefore, it appears that irrigation contributes to an increase in atmospheric moisture, and that a part of this moisture is recycled as continental precipitation, which can then be reevaporated.

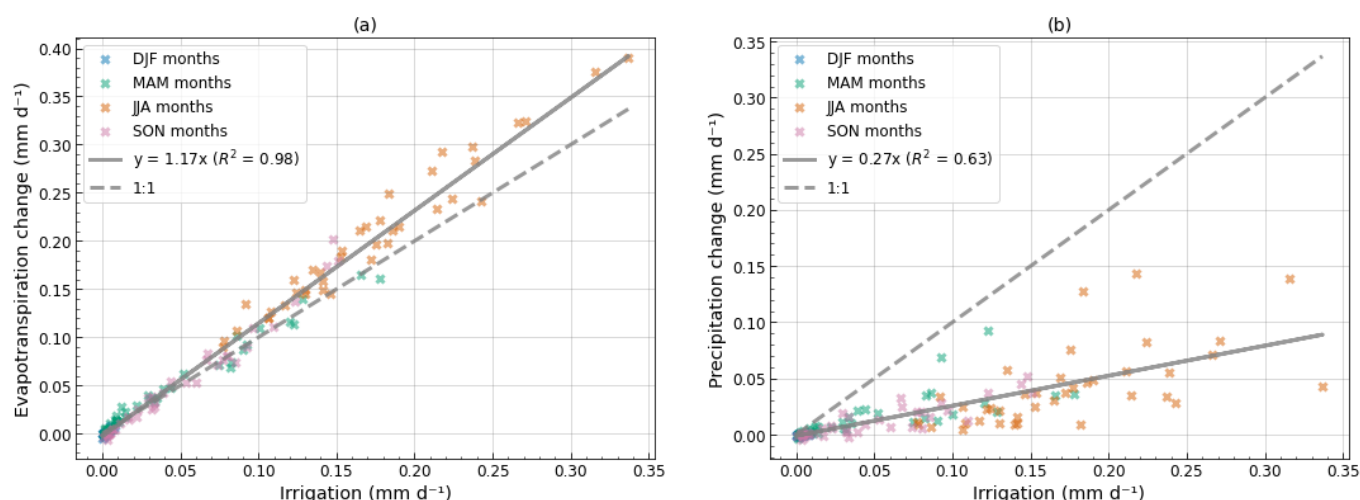


Figure 8. Domain-averaged influence of irrigation on monthly changes in ET and P (2010-2022). Each data point corresponds to the average value over the Iberian Peninsula continental domain for a single month of simulation (156 data points for 12 months over 13 years). The average amount of water added by irrigation in the *irr* simulation (mm d⁻¹) is plotted against the average change (*irr* - *no_irr*) in (a) ET (mm d⁻¹) and (b) P (mm d⁻¹). The data points for the winter months are all concentrated around (0,0) for both figures because of very small irrigation volumes and changes in ET and P during this season.

To look further into this recycling, three subdomains were defined, namely, low, medium and high irrigation areas, on the basis of the mean irrigation thresholds given in Table 4. In the map of simulated irrigation (Fig. 3d), the low irrigation domain corresponds to the first colour bin (yellow), the medium irrigation domain to the second bin (light green), and the high irrigation domain to the eight other bins. The three subdomains are also shown distinctly in Fig. 9e. On average, the increase in ET is slightly superior to irrigation for each subdomain (Fig. 9). However, the increase in precipitation is more than twice as large for the low irrigation subdomain than for the medium and high irrigation subdomains. Since irrigated areas are mostly in plains



and valleys, this result is consistent with the increase in precipitation already described over mountainous areas in summer (Fig. 7f). It points towards a nonlocal moisture recycling, with atmospheric moisture transfer from intensely irrigated areas to neighbouring lightly irrigated areas, meaning that a significant part of the additional rainfall does not occur on irrigated crops.

330 Over the entire Iberian Peninsula, the increase in precipitation represents 25 % of the irrigated volume, whereas the increase in ET amounts to 112 % of irrigation.

Table 4. Subdomains of different irrigation intensity.

Subdomain	Areal fraction (% of Iberian Peninsula)	Min. irrigation (mm d ⁻¹)	Max. irrigation (mm d ⁻¹)	Mean irrigation (mm d ⁻¹)
Low irrigation	56.3	0.0	0.06	0.033
Medium irrigation	34.0	0.06	0.12	0.082
High irrigation	9.7	0.12	0.61	0.210

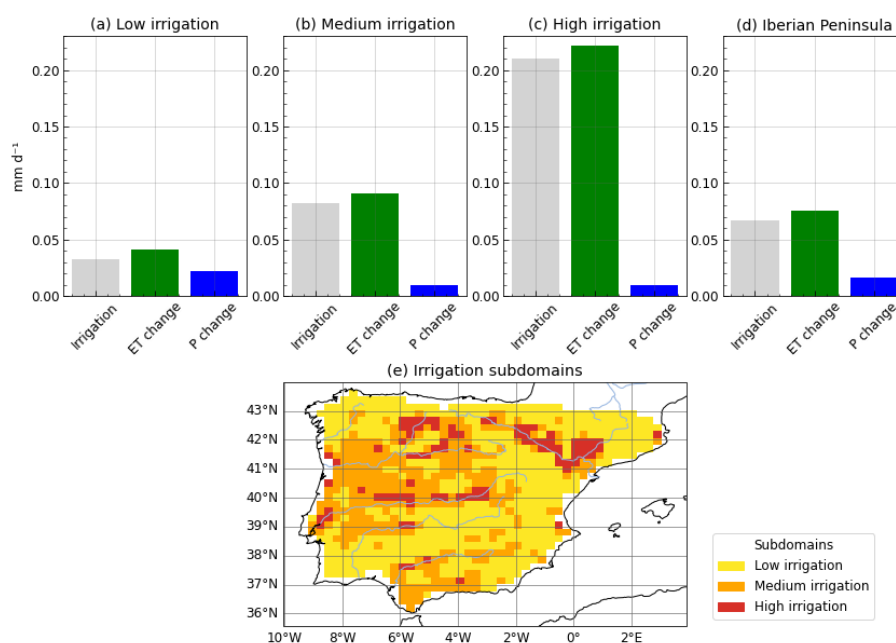


Figure 9. Changes in the atmospheric moisture budget for subdomains with different irrigation intensities. Each bar plot shows the annual mean irrigation in the *irr* simulation (2010-2022, mm d^{-1}) alongside the changes (*irr* - *no_irr*) in ET (mm d^{-1}) and P (mm d^{-1}) averaged over distinct subsets of the domain: (a) low irrigation, grid cells with an annual average irrigation lower than 0.06 mm d^{-1} , (b) medium irrigation, those where it is between 0.06 and 0.12 mm d^{-1} , (c) high irrigation those where it is higher than 0.12 mm d^{-1} , and (d) the Iberian Peninsula includes all 3 subsets. The three subdomains are shown in (e).



4 Discussion and conclusions

This study analyses the regional impacts of simulated irrigation on land surface-atmosphere coupling variables and the water cycle over the Iberian Peninsula. It uses a regional model at 25 km resolution, with the same physics as the global IPSL-CM, to better understand the strengths and limits of its parameterizations in representing the impacts of irrigation.

It first shows that the ORCHIDEE irrigation scheme simulates realistic values from April to September in areas where surface water withdrawals are most important, such as the Ebro Valley. However, it cannot represent winter irrigation, or satisfy irrigation demand in southern regions, where actual irrigation is more dependent on groundwater pumping and river dams, due to low available volumes in rivers and groundwater routing reservoirs. Ongoing developments to add river dams into the ORCHIDEE routing scheme (Baratgin et al., 2024) could very likely improve this aspect by representing interseasonal water storage, making more water available in summer. Explicit dam representation could also limit the winter and spring overestimates of river discharge in anthropized areas, since water would be stored in the dam reservoirs during this season instead of flowing in the rivers. Overall, the irrigation parameterization reduces river discharge and enables better agreement with observations, but since it is only active when the LAI is above a defined threshold, these impacts are mostly visible in summer and autumn. Future work with a looser activation threshold for irrigation could help to represent winter crop irrigation, although it is not expected to have as significant an impact on discharge as an explicit dam representation since simulated irrigation demand would still remain low in winter. Nevertheless, precipitation biases are very likely to remain a major driver of discharge biases, largely independent of irrigation or dam representation.

The simulation of precipitation and ET over the Iberian Peninsula is satisfactory in winter and spring, but this study highlights underestimates in summer and contrasted spatial patterns with positive precipitation biases in elevated regions and negative biases in plains. ET underestimation is partly improved by simulated irrigation, but remains present on average and over most of the domain. These linked biases might be improved with a different simulation setup, particularly in the lateral forcing. Preliminary analyses (not shown) revealed an abnormal behaviour of the model in the transition zone between the ERA5 forcing zone and the central free zone, which was attributed to discrepancies between the physics used in the model and in the reanalysis. This resulted in precipitation underestimations throughout the entire simulation domain, which were largely improved by using a larger domain for the simulations presented here. A good lead for future works would be to use lateral forcing from global simulations of the ICOLMDZ model or nested LAM simulations rather than a reanalysis, but these options are not yet technically available. The precipitation biases can also be due to structural flaws of the IPSL-CM parameterizations, as mentioned for mountain precipitation in Arjdal et al. (2024), and improving them might require more work in the modelling of radiative processes, shallow and deep convection (whose tuning often focuses on tropical regions), or surface processes (roughness, albedo, components of ET). This highlights the fact that the results of this study are necessarily limited by the modelling choices, uncertainties, and biases of the IPSL-CM, and therefore remain largely model-specific.

The atmospheric impacts of irrigation are analysed in more detail in summer, since it is the season with the largest irrigation values and the most significant response for all variables of interest, although it is the driest season, with very little precipitation. In JJA, the strong response of turbulent fluxes to irrigation leads to cooling and moistening of the lower atmosphere and signif-



icantly affects its structure (LCL and ABL height), with stronger effects on intensely irrigated regions, which is consistent with the findings of Rappin et al. (2022). In contrast, significant increases in precipitation are mostly detected in lightly irrigated mountainous areas surrounding the highly irrigated Ebro Valley. This points to a dominant effect of ABL stabilization, described by Findell and Eltahir (2003b); Ek and Holtslag (2004), in intensely irrigated areas, and remote effects of atmospheric moistening as in DeAngelis et al. (2010); Lo and Famiglietti (2013); Yang et al. (2017). An improved representation of winter and spring irrigation could either allow to generalize the following results or to identify different responses to irrigation under moister atmospheric conditions. Furthermore, over the Iberian Peninsula, increases in ET are proportional to applied irrigation and actually exceed it for almost every simulation month. This is made possible by small but systematic increases in average precipitation over the domain, forming evidence of continental moisture recycling over the Iberian Peninsula. The precipitation increases are of lower magnitude than those of ET and occur much more in lightly irrigated regions than in intensely irrigated regions, confirming that the recycling is partial and mostly nonlocal.

These findings call for an analysis of surface-atmosphere coupling processes in the presence of irrigation at the diurnal scale to better describe the impacts on the ABL structure in both irrigated areas and neighbouring regions. In particular, it would be relevant to compare the model to field observations from the LIAISE campaign held in the Ebro Valley in July 2021 (Boone et al., 2025). High resolution modelling experiments using irrigation parameterizations have shown large improvements of performance relative to LIAISE observations for turbulent fluxes, air temperature and humidity (Lunel et al., 2024a; Udina et al., 2024); stressed the importance of the convection parameterization for the response of precipitation to irrigation (Udina et al., 2024); and identified interactions of irrigation-induced heterogeneities with regional breeze circulations (Lunel et al., 2024b). Conducting similar analyses with the simulation setup used in this study should provide insights into the ability of an ESM to reproduce the complex structure of these heterogeneities (Mangan et al., 2023) and their impacts on the ABL and atmospheric water cycle.

<https://doi.org/10.5194/egusphere-2025-2491>

Preprint. Discussion started: 23 June 2025

© Author(s) 2025. CC BY 4.0 License.



Appendix A: River discharge

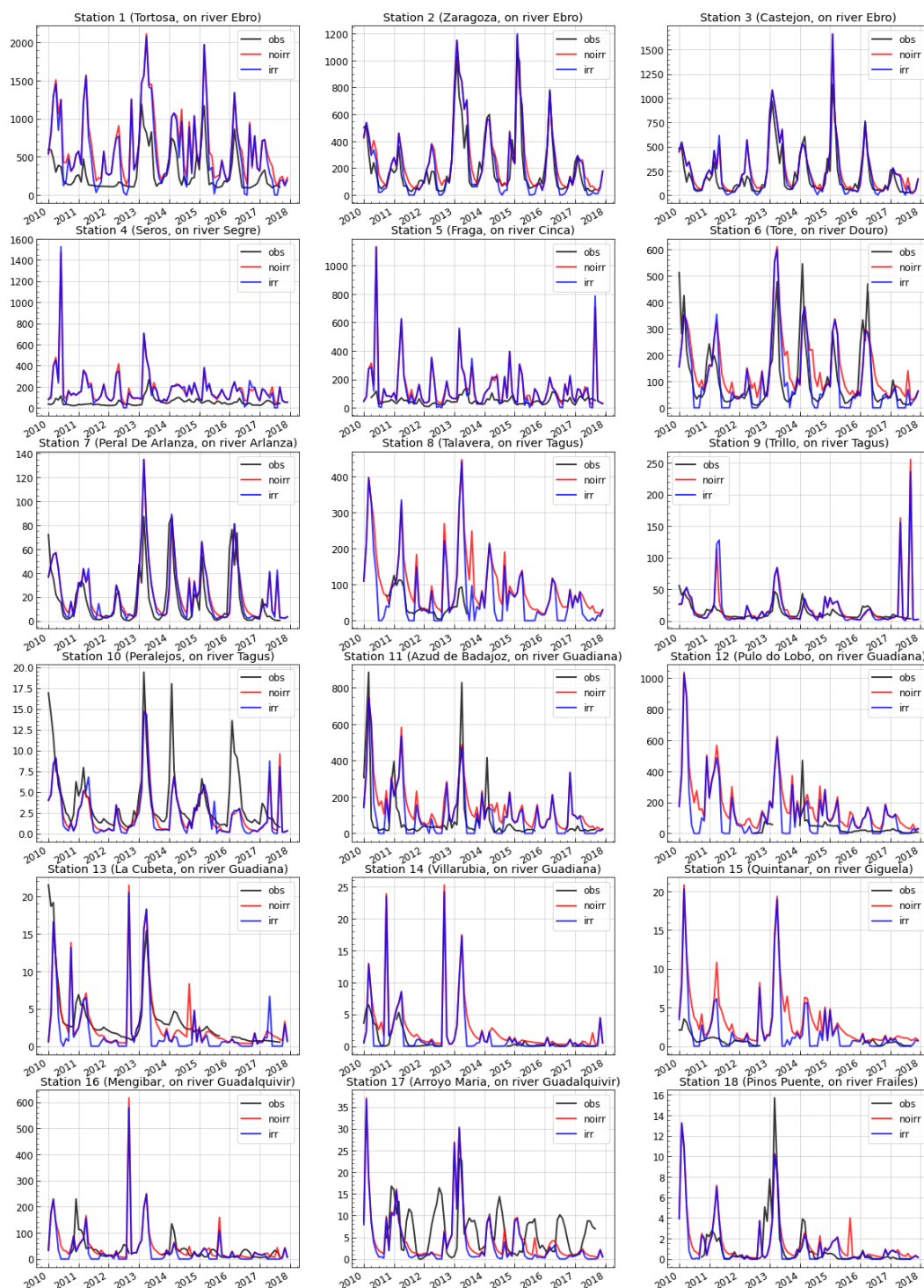


Figure A1. Time series of river discharge for the irr and no_irr simulations and GRDC observations.

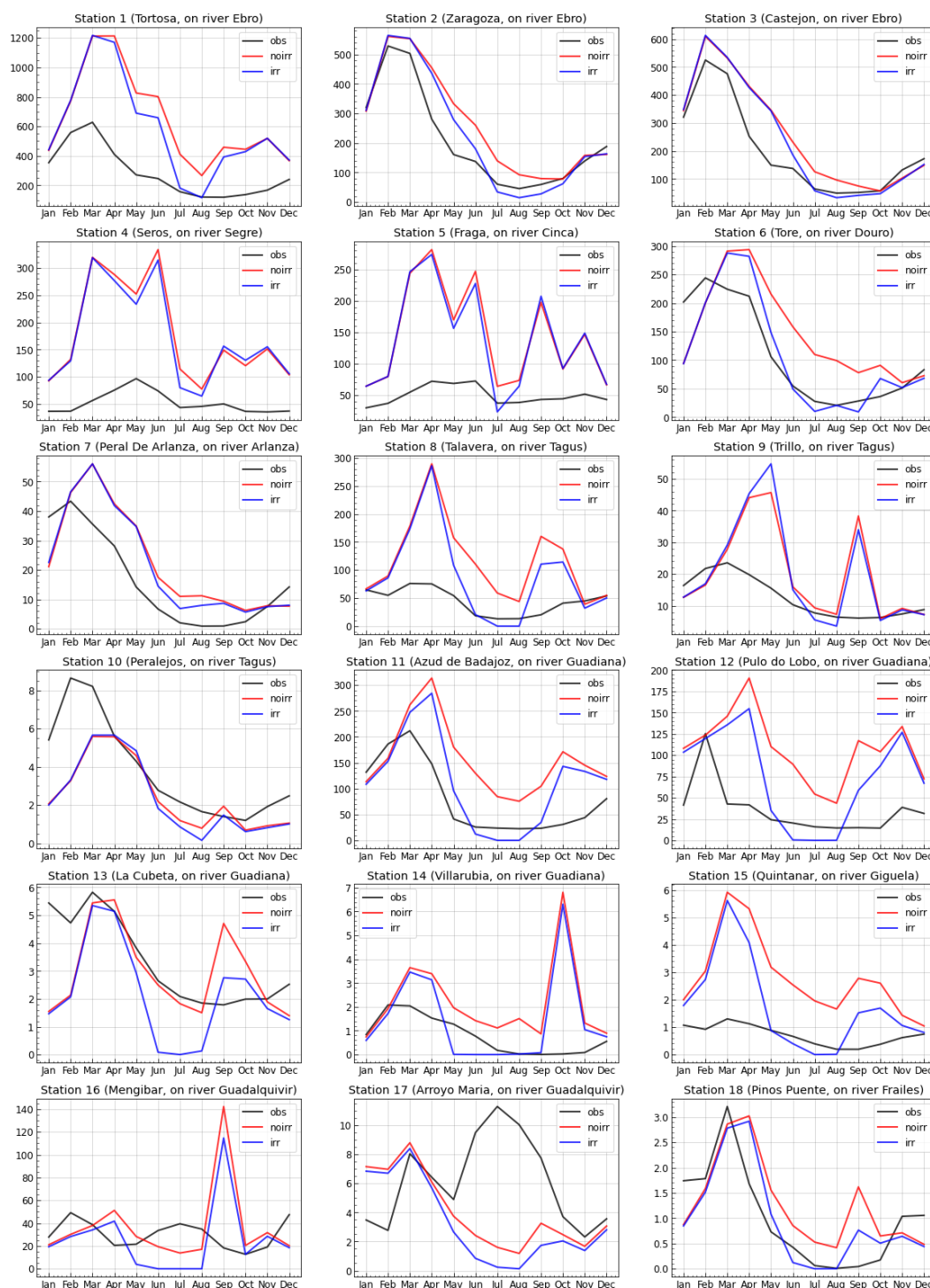


Figure A2. Mean seasonal cycle of river discharge for the *irr* and *noirr* simulations and GRDC observations. A mask is applied to the simulations to filter out months without corresponding observation data.



Code and data availability. The version of the ORCHIDEE LSM used for this study corresponds to tag 2.2, revision 8473 and is freely available from https://forge.ipsl.fr/orchidee/log/branches/ORCHIDEE_2_2. It is provided under a CeCILL-C license (French equivalent to the LGPL license). The LMDZ and DYNAMICO models are freely distributed at the following links <https://web.lmd.jussieu.fr/~lmdz/pub/> (revision 4507) and <https://gitlab.in2p3.fr/ipsl/projets/dynamico/dynamico> (revision 4501).

The Python code used to produce the figures and tables of this manuscript is available at https://github.com/ptiengou/netcdf-scripts/blob/main/python_notebooks/LMDZOR/LAM_06_article_figures.ipynb

The simulation outputs and observation data used are available at <https://doi.org/10.5281/zenodo.15704577>.

Author contributions. PT ran the simulations, conducted the analysis, produced the figures and wrote the manuscript. AD and FC supervised the research, guided the analysis, and edited the manuscript.

Competing interests. The authors declare no conflict of interest.

Acknowledgements. This work has received support from project BLUEGEM (grant no. ANR-21-SOIL-0001). The simulations were run using the IDRIS computational facilities (Institut du Développement et des Ressources en Informatique Scientifique, CNRS, France), under the allocations [AD010113599R1] and [A0150114642]. The authors acknowledge and thank Aurélien Baro (METIS GIS engineer) for editing Fig.2, Yann Meurdesoif and Antoine Bierjon for their assistance in running the LAM simulations with river routing and irrigation, as well as Julie Collignan for her help with river discharge observations. They also wish to thank Pedro Arboleda and Filipe Aires for helpful discussions while conducting the analysis.



References

- Adhikari, P., Geerts, B., Rahimi-Esfarjani, S., Smith, K., Shuman, B. N., and Schneider, T. L.: Evaluation of the Mountain Hydroclimate across the Western United States in Dynamically Downscaled Climate Models, <https://doi.org/10.1175/JHM-D-24-0063.1>, section: Journal of Hydrometeorology, 2024.
- 410 Al-Yaari, A., Ducharne, A., Cheruy, F., Crow, W. T., and Wigneron, J.-P.: Satellite-based soil moisture provides missing link between summertime precipitation and surface temperature biases in CMIP5 simulations over conterminous United States, *Sci Rep*, 9, 1657, <https://doi.org/10.1038/s41598-018-38309-5>, 2019.
- Al-Yaari, A., Ducharne, A., Thiery, W., Cheruy, F., and Lawrence, D.: The Role of Irrigation Expansion on Historical Climate Change: Insights From CMIP6, *Earth's Future*, 10, e2022EF002859, <https://doi.org/10.1029/2022EF002859>, _eprint: <https://onlinelibrary.wiley.com/doi/pdf/10.1029/2022EF002859>, 2022.
- 415 Alter, R. E., Im, E.-S., and Eltahir, E. A. B.: Rainfall consistently enhanced around the Gezira Scheme in East Africa due to irrigation, *Nature Geosci*, 8, 763–767, <https://doi.org/10.1038/ngeo2514>, number: 10 Publisher: Nature Publishing Group, 2015.
- Aquastat Geo-reference Database on Dams: <https://www.fao.org/aquastat/en/databases/dams>.
- Arboleda-Obando, P. F., Ducharne, A., Yin, Z., and Ciais, P.: Validation of a new global irrigation scheme in the land surface model ORCHIDEE v2.2, *Geoscientific Model Development*, 17, 2141–2164, <https://doi.org/10.5194/gmd-17-2141-2024>, publisher: Copernicus GmbH, 2024.
- Arjdal, K., Vignon, , Driouech, F., Chéruey, F., Er-Raki, S., Sima, A., Chehbouni, A., and Drobinski, P.: Modeling Land–Atmosphere Interactions over Semiarid Plains in Morocco: In-Depth Assessment of GCM Stretched-Grid Simulations Using In Situ Data, <https://doi.org/10.1175/JAMC-D-23-0099.1>, section: Journal of Applied Meteorology and Climatology, 2024.
- 425 Baratgin, L., Polcher, J., Dumas, P., and Quirion, P.: Modeling hydropower operations at the scale of a power grid: a demand-based approach, *Hydrology and Earth System Sciences*, 28, 5479–5509, <https://doi.org/10.5194/hess-28-5479-2024>, publisher: Copernicus GmbH, 2024.
- Berg, A., Lintner, B. R., Findell, K., Seneviratne, S. I., Hurk, B. v. d., Ducharne, A., Chéruey, F., Hagemann, S., Lawrence, D. M., Malyshev, S., Meier, A., and Gentine, P.: Interannual Coupling between Summertime Surface Temperature and Precipitation over Land: Processes and Implications for Climate Change, *Journal of Climate*, 28, 1308–1328, <https://doi.org/10.1175/JCLI-D-14-00324.1>, publisher: American Meteorological Society Section: Journal of Climate, 2015.
- 430 Betts, A. K. and Ball, J. H.: The FIFE surface diurnal cycle climate, *Journal of Geophysical Research: Atmospheres*, 100, 25 679–25 693, <https://doi.org/10.1029/94JD03121>, _eprint: <https://onlinelibrary.wiley.com/doi/pdf/10.1029/94JD03121>, 1995.
- Bonfils, C. and Lobell, D.: Empirical evidence for a recent slowdown in irrigation-induced cooling, *Proceedings of the National Academy of Sciences*, 104, 13 582–13 587, <https://doi.org/10.1073/pnas.0700144104>, publisher: Proceedings of the National Academy of Sciences, 435 2007.
- Boone, A., Bellvert, J., Best, M., Brooke, J. K., Canut-Rocafort, G., Cuxart, J., Hartogensis, O., Moigne, P. L., Miró, J. R., Polcher, J., Price, J., Seguí, P. Q., Bech, J., Bezombes, Y., Branch, O., Cristóbal, J., Dassas, K., Fanise, P., Gibert, F., Goulas, Y., Groh, J., Hanus, J., Hmimina, G., Jarlan, L., Kim, E., Dantec, V. L., Page, M. L., Lohou, F., Lothon, M., Mangan, M. R., Martí, B., Martínez-Villagrasa, D., McGregor, J., Kerr-Munslow, A., Ouadi, N., Philibert, A., Quiros-Vargas, J., Rascher, U., Siegmann, B., Udina, M., Vial, A., Wrenger, 440 B., Wulfmeyer, V., and Zribi, M.: The Land Surface Interactions with the Atmosphere over the Iberian Semi-Arid Environment (LIAISE) field campaign, *Journal of the European Meteorological Society*, 2, 100 007, <https://doi.org/10.1016/j.jemets.2025.100007>, 2025.



- Boone, A. A.: Land surface Interactions with the Atmosphere over the Iberian Semi-arid Environment (LIAISE), <https://hal.archives-ouvertes.fr/hal-02392949>, 2019.
- Boucher, O., Servonnat, J., Albright, A. L., Aumont, O., Balkanski, Y., Bastrikov, V., Bekki, S., Bonnet, R., Bony, S., Bopp, L., Braconnot, P., Brockmann, P., Cadule, P., Caubel, A., Cheruy, F., Codron, F., Cozic, A., Cugnet, D., D'Andrea, F., Davini, P., de Lavergne, C., Denvil, S., Deshayes, J., Devilliers, M., Ducharne, A., Dufresne, J.-L., Dupont, E., Éthé, C., Fairhead, L., Falletti, L., Flavoni, S., Foujols, M.-A., Gardoll, S., Gastineau, G., Ghattas, J., Grandpeix, J.-Y., Guenet, B., Guez, Lionel, E., Guilyardi, E., Guimberteau, M., Hauglustaine, D., Hourdin, F., Idelkadi, A., Joussaume, S., Kageyama, M., Khodri, M., Krinner, G., Lebas, N., Levavasseur, G., Lévy, C., Li, L., Lott, F., Lurton, T., Luyssaert, S., Madec, G., Madeleine, J.-B., Maignan, F., Marchand, M., Marti, O., Mellul, L., Meurdesoif, Y., Mignot, J., Musat, I., Ottlé, C., Peylin, P., Planton, Y., Polcher, J., Rio, C., Rochetin, N., Rousset, C., Sepulchre, P., Sima, A., Swingedouw, D., Thiéblemont, R., Traore, A. K., Vancoppenolle, M., Vial, J., Vialard, J., Viovy, N., and Vuichard, N.: Presentation and Evaluation of the IPSL-CM6A-LR Climate Model, *Journal of Advances in Modeling Earth Systems*, 12, e2019MS002 010, <https://doi.org/10.1029/2019MS002010>, <https://onlinelibrary.wiley.com/doi/pdf/10.1029/2019MS002010>, 2020.
- Budyko, M. and Miller, D.: *Climate and Life*. Academic Press, New York, 1974.
- Budyko, M. I.: *The heat balance of the earth's surface*, 1956.
- Cheruy, F., Campoy, A., Dupont, J.-C., Ducharne, A., Hourdin, F., Haefelin, M., Chiriaco, M., and Idelkadi, A.: Combined influence of atmospheric physics and soil hydrology on the simulated meteorology at the SIRTa atmospheric observatory, *Clim Dyn*, 40, 2251–2269, <https://doi.org/10.1007/s00382-012-1469-y>, 2013.
- Cheruy, F., Dufresne, J. L., Hourdin, F., and Ducharne, A.: Role of clouds and land-atmosphere coupling in midlatitude continental summer warm biases and climate change amplification in CMIP5 simulations, *Geophys. Res. Lett.*, 41, 6493–6500, <https://doi.org/10.1002/2014GL061145>, 2014.
- Cheruy, F., Ducharne, A., Hourdin, F., Musat, I., Vignon, , Gastineau, G., Bastrikov, V., Vuichard, N., Diallo, B., Dufresne, J., Ghattas, J., Grandpeix, J., Idelkadi, A., Mellul, L., Maignan, F., Ménégos, M., Ottlé, C., Peylin, P., Servonnat, J., Wang, F., and Zhao, Y.: Improved Near-Surface Continental Climate in IPSL-CM6A-LR by Combined Evolutions of Atmospheric and Land Surface Physics, *J Adv Model Earth Syst*, 12, <https://doi.org/10.1029/2019MS002005>, 2020.
- Christensen, J. H. and Boberg, F.: Temperature dependent climate projection deficiencies in CMIP5 models, *Geophysical Research Letters*, 39, <https://doi.org/10.1029/2012GL053650>, [eprint: https://onlinelibrary.wiley.com/doi/pdf/10.1029/2012GL053650](https://onlinelibrary.wiley.com/doi/pdf/10.1029/2012GL053650), 2012.
- Cook, B. I., Shukla, S. P., Puma, M. J., and Nazarenko, L. S.: Irrigation as an historical climate forcing, *Clim Dyn*, 44, 1715–1730, <https://doi.org/10.1007/s00382-014-2204-7>, 2015.
- Custodio, E., Andreu-Rodes, J. M., Aragón, R., Estrela, T., Ferrer, J., García-Aróstegui, J. L., Manzano, M., Rodríguez-Hernández, L., Sahuquillo, A., and del Villar, A.: Groundwater intensive use and mining in south-eastern peninsular Spain: Hydrogeological, economic and social aspects, *Science of The Total Environment*, 559, 302–316, <https://doi.org/10.1016/j.scitotenv.2016.02.107>, 2016.
- Dari, J., Brocca, L., Modanesi, S., Massari, C., Tarpanelli, A., Barbetta, S., Quast, R., Vreugdenhil, M., Freeman, V., Barella-Ortiz, A., Quintana-Seguí, P., Bretreger, D., and Volden, E.: Regional data sets of high-resolution (1 and 6 km) irrigation estimates from space, *Earth System Science Data*, 15, 1555–1575, <https://doi.org/10.5194/essd-15-1555-2023>, publisher: Copernicus GmbH, 2023.
- de Vrese, P., Hagemann, S., and Claussen, M.: Asian irrigation, African rain: Remote impacts of irrigation, *Geophysical Research Letters*, 43, 3737–3745, <https://doi.org/10.1002/2016GL068146>, [eprint: https://onlinelibrary.wiley.com/doi/pdf/10.1002/2016GL068146](https://onlinelibrary.wiley.com/doi/pdf/10.1002/2016GL068146), 2016.



- DeAngelis, A., Dominguez, F., Fan, Y., Robock, A., Kustu, M. D., and Robinson, D.: Evidence of enhanced precipitation due to irrigation over the Great Plains of the United States, *Journal of Geophysical Research: Atmospheres*, 115, <https://doi.org/10.1029/2010JD013892>,
480 _eprint: <https://onlinelibrary.wiley.com/doi/pdf/10.1029/2010JD013892>, 2010.
- Dirmeyer, P. A.: The terrestrial segment of soil moisture–climate coupling, *Geophysical Research Letters*, 38, <https://doi.org/10.1029/2011GL048268>, _eprint: <https://onlinelibrary.wiley.com/doi/pdf/10.1029/2011GL048268>, 2011.
- Dubos, T., Dubey, S., Tort, M., Mittal, R., Meurdesoif, Y., and Hourdin, F.: DYNAMICO-1.0, an icosahedral hydrostatic dynamical core designed for consistency and versatility, *Geoscientific Model Development*, 8, 3131–3150, <https://doi.org/10.5194/gmd-8-3131-2015>,
485 publisher: Copernicus GmbH, 2015.
- Ek, M. B. and Holtslag, A. A. M.: Influence of Soil Moisture on Boundary Layer Cloud Development, *J. Hydrometeor*, 5, 86–99, [https://doi.org/10.1175/1525-7541\(2004\)005<0086:IOSMOB>2.0.CO;2](https://doi.org/10.1175/1525-7541(2004)005<0086:IOSMOB>2.0.CO;2), 2004.
- Eltahir, E. A. B. and Bras, R. L.: Precipitation recycling, *Reviews of Geophysics*, 34, 367–378, <https://doi.org/10.1029/96RG01927>, _eprint: <https://onlinelibrary.wiley.com/doi/pdf/10.1029/96RG01927>, 1996.
- 490 Emanuel, K. A.: A Scheme for Representing Cumulus Convection in Large-Scale Models, https://journals.ametsoc.org/view/journals/atsc/48/21/1520-0469_1991_048_2313_asfrcc_2_0_co_2.xml, section: *Journal of the Atmospheric Sciences*, 1991.
- Farran, F. C.: The Urgell canal, a human miracle, *Per saber-ne m{\`e}s*, 2024.
- Fekete, B. M.: Global, Composite Runoff Fields Based on Observed River Discharge and Simulated Water Balances., <https://doi.org/10.1594/PANGAEA.97167>, accepted: 2019-11-26T04:00:25Z *Journal Abbreviation: Danube river, Ceatal Izmail, monthly*
495 *min-mean-max discharge, 1921-1984*, 2003.
- Findell, K. L. and Eltahir, E. A. B.: Atmospheric controls on soil moisture–boundary layer interactions: Three-dimensional wind effects, *Journal of Geophysical Research: Atmospheres*, 108, <https://doi.org/10.1029/2001JD001515>, _eprint: <https://onlinelibrary.wiley.com/doi/pdf/10.1029/2001JD001515>, 2003a.
- Findell, K. L. and Eltahir, E. A. B.: Atmospheric Controls on Soil Moisture–Boundary Layer Interactions. Part II: Feedbacks within the Continental United States, *Journal of Hydrometeorology*, 4, 570–583, [https://doi.org/10.1175/1525-7541\(2003\)004<0570:ACOSML>2.0.CO;2](https://doi.org/10.1175/1525-7541(2003)004<0570:ACOSML>2.0.CO;2),
500 publisher: American Meteorological Society Section: *Journal of Hydrometeorology*, 2003b.
- Findell, K. L., Gentine, P., Lintner, B. R., and Kerr, C.: Probability of afternoon precipitation in eastern United States and Mexico enhanced by high evaporation, *Nature Geosci*, 4, 434–439, <https://doi.org/10.1038/ngeo1174>, number: 7 Publisher: Nature Publishing Group, 2011.
- Grandpeix, J.-Y. and Lafore, J.-P.: A Density Current Parameterization Coupled with Emanuel’s Convection Scheme. Part I: The Models, <https://doi.org/10.1175/2009JAS3044.1>, section: *Journal of the Atmospheric Sciences*, 2010.
505
- Grandpeix, J.-Y., Phillips, V., and Tailleux, R.: Improved mixing representation in Emanuel’s convection scheme, *Quarterly Journal of the Royal Meteorological Society*, 130, 3207–3222, <https://doi.org/10.1256/qj.03.144>, _eprint: <https://onlinelibrary.wiley.com/doi/pdf/10.1256/qj.03.144>, 2004.
- Grandpeix, J.-Y., Lafore, J.-P., and Cheruy, F.: A Density Current Parameterization Coupled with Emanuel’s Convection Scheme. Part II: 1D
510 Simulations, <https://doi.org/10.1175/2009JAS3045.1>, section: *Journal of the Atmospheric Sciences*, 2010.
- Guillod, B. P., Orlowsky, B., Miralles, D. G., Teuling, A. J., and Seneviratne, S. I.: Reconciling spatial and temporal soil moisture effects on afternoon rainfall, *Nat Commun*, 6, 6443, <https://doi.org/10.1038/ncomms7443>, number: 1 Publisher: Nature Publishing Group, 2015.
- Guo, Z., Dirmeyer, P. A., Koster, R. D., Sud, Y. C., Bonan, G., Oleson, K. W., Chan, E., Verseghy, D., Cox, P., Gordon, C. T., McGregor, J. L., Kanae, S., Kowalczyk, E., Lawrence, D., Liu, P., Mocko, D., Lu, C.-H., Mitchell, K., Malyshev, S., McAvaney, B., Oki, T., Yamada,



- 515 T., Pitman, A., Taylor, C. M., Vasic, R., and Xue, Y.: GLACE: The Global Land–Atmosphere Coupling Experiment. Part II: Analysis, *Journal of Hydrometeorology*, 7, 611–625, <https://doi.org/10.1175/JHM511.1>, 2006.
- Hersbach, H., Bell, B., Berrisford, P., Hirahara, S., Horányi, A., Muñoz-Sabater, J., Nicolas, J., Peubey, C., Radu, R., Schepers, D., Simmons, A., Soci, C., Abdalla, S., Abellan, X., Balsamo, G., Bechtold, P., Biavati, G., Bidlot, J., Bonavita, M., De Chiara, G., Dahlgren, P., Dee, D., Diamantakis, M., Dragani, R., Flemming, J., Forbes, R., Fuentes, M., Geer, A., Haimberger, L., Healy, S., Hogan, R. J.,
520 Hólm, E., Janisková, M., Keeley, S., Laloyaux, P., Lopez, P., Lupu, C., Radnoti, G., de Rosnay, P., Rozum, I., Vamborg, F., Villaume, S., and Thépaut, J.-N.: The ERA5 global reanalysis, *Quarterly Journal of the Royal Meteorological Society*, 146, 1999–2049, <https://doi.org/10.1002/qj.3803>, _eprint: <https://onlinelibrary.wiley.com/doi/pdf/10.1002/qj.3803>, 2020.
- Hourdin, F., Jam, A., Rio, C., Couvreur, F., Sandu, I., Lefebvre, M.-P., Brient, F., and Idelkadi, A.: Unified Parameterization of Convective Boundary Layer Transport and Clouds With the Thermal Plume Model, *Journal of Advances in Modeling Earth Systems*, 11, 2910–2933,
525 <https://doi.org/10.1029/2019MS001666>, _eprint: <https://onlinelibrary.wiley.com/doi/pdf/10.1029/2019MS001666>, 2019.
- Hourdin, F., Rio, C., Grandpeix, J.-Y., Madeleine, J.-B., Cheruy, F., Rochetin, N., Jam, A., Musat, I., Idelkadi, A., Fairhead, L., Foujols, M.-A., Mellul, L., Traore, A.-K., Dufresne, J.-L., Boucher, O., Lefebvre, M.-P., Millour, E., Vignon, E., Jouhaud, J., Diallo, F. B., Lott, F., Gastineau, G., Caubel, A., Meurdesoif, Y., and Ghattas, J.: LMDZ6A: The Atmospheric Component of the IPSL Climate Model With Improved and Better Tuned Physics, *Journal of Advances in Modeling Earth Systems*, 12, e2019MS001892,
530 <https://doi.org/10.1029/2019MS001892>, _eprint: <https://onlinelibrary.wiley.com/doi/pdf/10.1029/2019MS001892>, 2020.
- Hurt, G. C., Chini, L., Sahajpal, R., Frolking, S., Bodirsky, B. L., Calvin, K., Doelman, J. C., Fisk, J., Fujimori, S., Klein Goldewijk, K., Hasegawa, T., Havlik, P., Heinemann, A., Humpenöder, F., Jungclaus, J., Kaplan, J. O., Kennedy, J., Krisztin, T., Lawrence, D., Lawrence, P., Ma, L., Mertz, O., Pongratz, J., Popp, A., Poulter, B., Riahi, K., Shevliakova, E., Stehfest, E., Thornton, P., Tubiello, F. N., van Vuuren, D. P., and Zhang, X.: Harmonization of global land use change and management for the period 850–2100 (LUH2) for CMIP6,
535 *Geoscientific Model Development*, 13, 5425–5464, <https://doi.org/10.5194/gmd-13-5425-2020>, publisher: Copernicus GmbH, 2020.
- King, J. C., Connolley, W. M., and Derbyshire, S. H.: Sensitivity of modelled Antarctic climate to surface and boundary-layer flux parametrizations, *Quarterly Journal of the Royal Meteorological Society*, 127, 779–794, <https://doi.org/10.1002/qj.49712757304>, _eprint: <https://onlinelibrary.wiley.com/doi/pdf/10.1002/qj.49712757304>, 2001.
- Klein, C. and Taylor, C. M.: Dry soils can intensify mesoscale convective systems, *Proceedings of the National Academy of Sciences*, 117,
540 21 132–21 137, <https://doi.org/10.1073/pnas.2007998117>, publisher: Proceedings of the National Academy of Sciences, 2020.
- Koster, R. D., Suarez, M. J., Higgins, R. W., and Van den Dool, H. M.: Observational evidence that soil moisture variations affect precipitation, *Geophysical Research Letters*, 30, <https://doi.org/10.1029/2002GL016571>, _eprint: <https://onlinelibrary.wiley.com/doi/pdf/10.1029/2002GL016571>, 2003.
- Koster, R. D., Dirmeyer, P. A., Guo, Z., Bonan, G., Chan, E., Cox, P., Gordon, C. T., Kanae, S., Kowalczyk, E., Lawrence, D., Liu, P., Lu, C.-H., Malyshev, S., McAvaney, B., Mitchell, K., Mocko, D., Oki, T., Oleson, K., Pitman, A., Sud, Y. C., Taylor, C. M., Verseghy, D.,
545 Vasic, R., Xue, Y., and Yamada, T.: Regions of Strong Coupling Between Soil Moisture and Precipitation, *Science*, 305, 1138–1140, <https://doi.org/10.1126/science.1100217>, publisher: American Association for the Advancement of Science, 2004.
- Krinner, G., Viovy, N., de Noblet-Ducoudré, N., Ogée, J., Polcher, J., Friedlingstein, P., Ciais, P., Sitch, S., and Prentice, I. C.: A dynamic global vegetation model for studies of the coupled atmosphere-biosphere system, *Global Biogeochemical Cycles*, 19,
550 <https://doi.org/10.1029/2003GB002199>, _eprint: <https://onlinelibrary.wiley.com/doi/pdf/10.1029/2003GB002199>, 2005.



- Leng, G., Leung, L. R., and Huang, M.: Significant impacts of irrigation water sources and methods on modeling irrigation effects in the ACME Land Model, *Journal of Advances in Modeling Earth Systems*, 9, 1665–1683, <https://doi.org/10.1002/2016MS000885>, [_eprint: https://onlinelibrary.wiley.com/doi/pdf/10.1002/2016MS000885](https://onlinelibrary.wiley.com/doi/pdf/10.1002/2016MS000885), 2017.
- Lo, M.-H. and Famiglietti, J. S.: Irrigation in California’s Central Valley strengthens the southwestern U.S. water cycle, *Geophysical Research Letters*, 40, 301–306, <https://doi.org/10.1002/grl.50108>, [_eprint: https://onlinelibrary.wiley.com/doi/pdf/10.1002/grl.50108](https://onlinelibrary.wiley.com/doi/pdf/10.1002/grl.50108), 2013.
- Lo, M.-H., Wey, H.-W., Im, E.-S., Tang, L. I., Anderson, R. G., Wu, R.-J., Chien, R.-Y., Wei, J., AghaKouchak, A., and Wada, Y.: Intense agricultural irrigation induced contrasting precipitation changes in Saudi Arabia, *Environ. Res. Lett.*, 16, 064049, <https://doi.org/10.1088/1748-9326/ac002e>, publisher: IOP Publishing, 2021.
- Lobera, G., Besné, P., Vericat, D., López-Tarazón, J. A., Tena, A., Aristi, I., Díez, J. R., Ibisate, A., Larrañaga, A., Elosegí, A., and Batalla, R. J.: Geomorphic status of regulated rivers in the Iberian Peninsula, *Sci Total Environ*, 508, 101–114, <https://doi.org/10.1016/j.scitotenv.2014.10.058>, 2015.
- Louis, J.-F.: A parametric model of vertical eddy fluxes in the atmosphere, *Boundary-Layer Meteorol*, 17, 187–202, <https://doi.org/10.1007/BF00117978>, 1979.
- Lunel, T., Boone, A. A., and Le Moigne, P.: Irrigation strongly influences near-surface conditions and induces breeze circulation: Observational and model-based evidence, *Quarterly Journal of the Royal Meteorological Society*, 150, 2798–2819, <https://doi.org/10.1002/qj.4736>, [_eprint: https://onlinelibrary.wiley.com/doi/pdf/10.1002/qj.4736](https://onlinelibrary.wiley.com/doi/pdf/10.1002/qj.4736), 2024a.
- Lunel, T., Jimenez, M. A., Cuxart, J., Martinez-Villagrasa, D., Boone, A., and Le Moigne, P.: The *marinada* fall wind in the eastern Ebro sub-basin: physical mechanisms and role of the sea, orography and irrigation, *Atmospheric Chemistry and Physics*, 24, 7637–7666, <https://doi.org/10.5194/acp-24-7637-2024>, publisher: Copernicus GmbH, 2024b.
- Lurton, T., Balkanski, Y., Bastrikov, V., Bekki, S., Bopp, L., Braconnot, P., Brockmann, P., Cadule, P., Contoux, C., Cozic, A., Cugnet, D., Dufresne, J.-L., Éthé, C., Foujols, M.-A., Ghattas, J., Hauglustaine, D., Hu, R.-M., Kageyama, M., Khodri, M., Lebas, N., Levavasseur, G., Marchand, M., Ottlé, C., Peylin, P., Sima, A., Szopa, S., Thiéblemont, R., Vuichard, N., and Boucher, O.: Implementation of the CMIP6 Forcing Data in the IPSL-CM6A-LR Model, *Journal of Advances in Modeling Earth Systems*, 12, e2019MS001940, <https://doi.org/10.1029/2019MS001940>, [_eprint: https://onlinelibrary.wiley.com/doi/pdf/10.1029/2019MS001940](https://onlinelibrary.wiley.com/doi/pdf/10.1029/2019MS001940), 2020.
- Madeleine, J.-B., Hourdin, F., Grandpeix, J.-Y., Rio, C., Dufresne, J.-L., Vignon, E., Boucher, O., Konsta, D., Cheruy, F., Musat, I., Idelkadi, A., Fairhead, L., Millour, E., Lefebvre, M.-P., Mellul, L., Rochetin, N., Lemonnier, F., Touzé-Peiffer, L., and Bonazzola, M.: Improved Representation of Clouds in the Atmospheric Component LMDZ6A of the IPSL-CM6A Earth System Model, *Journal of Advances in Modeling Earth Systems*, 12, e2020MS002046, <https://doi.org/10.1029/2020MS002046>, [_eprint: https://onlinelibrary.wiley.com/doi/pdf/10.1029/2020MS002046](https://onlinelibrary.wiley.com/doi/pdf/10.1029/2020MS002046), 2020.
- Mangan, M. R., Hartogensis, O., Boone, A., Branch, O., Canut, G., Cuxart, J., de Boer, H. J., Le Page, M., Martínez-Villagrasa, D., Miró, J. R., Price, J., and Vilà-Guerau de Arellano, J.: The surface-boundary layer connection across spatial scales of irrigation-driven thermal heterogeneity: An integrated data and modeling study of the LIAISE field campaign, *Agricultural and Forest Meteorology*, 335, 109452, <https://doi.org/10.1016/j.agrformet.2023.109452>, 2023.
- Martens, B., Miralles, D. G., Lievens, H., van der Schalie, R., de Jeu, R. A. M., Fernández-Prieto, D., Beck, H. E., Dorigo, W. A., and Verhoest, N. E. C.: GLEAM v3: satellite-based land evaporation and root-zone soil moisture, *Geoscientific Model Development*, 10, 1903–1925, <https://doi.org/10.5194/gmd-10-1903-2017>, publisher: Copernicus GmbH, 2017.
- McDermid, S., Nocco, M., Lawston-Parker, P., Keune, J., Pokhrel, Y., Jain, M., Jägermeyr, J., Brocca, L., Massari, C., Jones, A. D., Vahmani, P., Thiery, W., Yao, Y., Bell, A., Chen, L., Dorigo, W., Hanasaki, N., Jasechko, S., Lo, M.-H., Mahmood, R., Mishra, V., Mueller,



- 590 N. D., Niyogi, D., Rabin, S. S., Sloat, L., Wada, Y., Zappa, L., Chen, F., Cook, B. I., Kim, H., Lombardozzi, D., Polcher, J., Ryu, D., Santanello, J., Satoh, Y., Seneviratne, S., Singh, D., and Yokohata, T.: Irrigation in the Earth system, *Nat Rev Earth Environ*, 4, 435–453, <https://doi.org/10.1038/s43017-023-00438-5>, number: 7 Publisher: Nature Publishing Group, 2023.
- Miralles, D. G., Bonte, O., Koppa, A., Baez-Villanueva, O. M., Tronquo, E., Zhong, F., Beck, H. E., Hulsman, P., Dorigo, W., Verhoest, N. E. C., and Haghdoust, S.: GLEAM4: global land evaporation and soil moisture dataset at 0.1° resolution from 1980 to near present, *Sci Data*, 12, 416, <https://doi.org/10.1038/s41597-025-04610-y>, publisher: Nature Publishing Group, 2025.
- 595 Mlawer, E. J., Taubman, S. J., Brown, P. D., Iacono, M. J., and Clough, S. A.: Radiative transfer for inhomogeneous atmospheres: RRTM, a validated correlated-k model for the longwave, *Journal of Geophysical Research: Atmospheres*, 102, 16 663–16 682, <https://doi.org/10.1029/97JD00237>, _eprint: <https://onlinelibrary.wiley.com/doi/pdf/10.1029/97JD00237>, 1997.
- Morán-Tejeda, E., Lorenzo-Lacruz, J., López-Moreno, J. I., Ceballos-Barbancho, A., Zabalza, J., and Vicente-Serrano, S. M.: Reservoir Management in the Duero Basin (Spain): Impact on River Regimes and the Response to Environmental Change, *Water Resour Manage*, 600 26, 2125–2146, <https://doi.org/10.1007/s11269-012-0004-6>, 2012.
- Mueller, B. and Seneviratne, S. I.: Systematic land climate and evapotranspiration biases in CMIP5 simulations, *Geophysical Research Letters*, 41, 128–134, <https://doi.org/10.1002/2013GL058055>, _eprint: <https://onlinelibrary.wiley.com/doi/pdf/10.1002/2013GL058055>, 2014.
- Ngo-Duc, T., Laval, K., Ramillien, G., Polcher, J., and Cazenave, A.: Validation of the land water storage simulated by Organising Carbon and Hydrology in Dynamic Ecosystems (ORCHIDEE) with Gravity Recovery and Climate Experiment (GRACE) data, *Water Resources Research*, 43, <https://doi.org/10.1029/2006WR004941>, _eprint: <https://onlinelibrary.wiley.com/doi/pdf/10.1029/2006WR004941>, 2007.
- 605 Nocco, M. A., Smail, R. A., and Kucharik, C. J.: Observation of irrigation-induced climate change in the Midwest United States, *Global Change Biology*, 25, 3472–3484, <https://doi.org/10.1111/gcb.14725>, _eprint: <https://onlinelibrary.wiley.com/doi/pdf/10.1111/gcb.14725>, 2019.
- 610 Phillips, C. E., Nair, U. S., Mahmood, R., Rappin, E., and Pielke Sr, R. A.: Influence of Irrigation on Diurnal Mesoscale Circulations: Results From GRAINEX, *Geophysical Research Letters*, 49, e2021GL096 822, <https://doi.org/10.1029/2021GL096822>, _eprint: <https://onlinelibrary.wiley.com/doi/pdf/10.1029/2021GL096822>, 2022.
- Pokhrel, Y., Hanasaki, N., Koirala, S., Cho, J., Yeh, P. J.-F., Kim, H., Kanae, S., and Oki, T.: Incorporating Anthropogenic Water Regulation Modules into a Land Surface Model, *Journal of Hydrometeorology*, 13, 255–269, <https://doi.org/10.1175/JHM-D-11-013.1>, publisher: American Meteorological Society Section: *Journal of Hydrometeorology*, 2012.
- 615 Polcher, J., Schrapffer, A., Dupont, E., Rinchiuso, L., Zhou, X., Boucher, O., Mouche, E., Ottlé, C., and Servonnat, J.: Hydrological modelling on atmospheric grids: using graphs of sub-grid elements to transport energy and water, *Geoscientific Model Development*, 16, 2583–2606, <https://doi.org/10.5194/gmd-16-2583-2023>, publisher: Copernicus GmbH, 2023.
- Puma, M. J. and Cook, B. I.: Effects of irrigation on global climate during the 20th century, *Journal of Geophysical Research: Atmospheres*, 620 115, <https://doi.org/10.1029/2010JD014122>, _eprint: <https://onlinelibrary.wiley.com/doi/pdf/10.1029/2010JD014122>, 2010.
- Raillard, L., Vignon, , Rivière, G., Madeleine, J.-B., Meurdesoif, Y., Delanoë, J., Caubel, A., Jourdan, O., Baudoux, A., Fromang, S., and Conesa, P.: Leveraging RALI-THINICE Observations to Assess How the ICOLMDZ Model Simulates Clouds Embedded in Arctic Cyclones, *Journal of Geophysical Research: Atmospheres*, 129, e2024JD040 973, <https://doi.org/10.1029/2024JD040973>, _eprint: <https://onlinelibrary.wiley.com/doi/pdf/10.1029/2024JD040973>, 2024.
- 625 Rappin, E., Mahmood, R., Nair, U., Pielke, R. A., Brown, W., Oncley, S., Wurman, J., Kosiba, K., Kaulfus, A., Phillips, C., Lachenmeier, E., Santanello, J., Kim, E., and Lawston-Parker, P.: The Great Plains Irrigation Experiment (GRAINEX), *Bulletin of the American Meteoro-*



- rological Society, 102, E1756–E1785, <https://doi.org/10.1175/BAMS-D-20-0041.1>, publisher: American Meteorological Society Section: Bulletin of the American Meteorological Society, 2021.
- 630 Rappin, E. D., Mahmood, R., Nair, U. S., and Sr, R. A. P.: Land–Atmosphere Interactions during GRAINEX: Planetary Boundary Layer Evolution in the Presence of Irrigation, *Journal of Hydrometeorology*, 23, 1401–1417, <https://doi.org/10.1175/JHM-D-21-0160.1>, publisher: American Meteorological Society Section: Journal of Hydrometeorology, 2022.
- Reynolds, C. A., Jackson, T. J., and Rawls, W. J.: Estimating soil water-holding capacities by linking the Food and Agriculture Organization Soil map of the world with global pedon databases and continuous pedotransfer functions, *Water Resources Research*, 36, 3653–3662, <https://doi.org/10.1029/2000WR900130>, eprint: <https://onlinelibrary.wiley.com/doi/pdf/10.1029/2000WR900130>, 2000.
- 635 Rio, C. and Hourdin, F.: A Thermal Plume Model for the Convective Boundary Layer: Representation of Cumulus Clouds, <https://doi.org/10.1175/2007JAS2256.1>, section: Journal of the Atmospheric Sciences, 2008.
- Rio, C., Grandpeix, J.-Y., Hourdin, F., Guichard, F., Couvreux, F., Lafore, J.-P., Fridlind, A., Mrowiec, A., Roehrig, R., Rochetin, N., Lefebvre, M.-P., and Idelkadi, A.: Control of deep convection by sub-cloud lifting processes: the ALP closure in the LMDZ5B general circulation model, *Clim Dyn*, 40, 2271–2292, <https://doi.org/10.1007/s00382-012-1506-x>, 2013.
- 640 Rochetin, N., Couvreux, F., Grandpeix, J.-Y., and Rio, C.: Deep Convection Triggering by Boundary Layer Thermals. Part I: LES Analysis and Stochastic Triggering Formulation, *Journal of the Atmospheric Sciences*, 71, 496–514, <https://doi.org/10.1175/JAS-D-12-0336.1>, publisher: American Meteorological Society Section: Journal of the Atmospheric Sciences, 2014a.
- Rochetin, N., Grandpeix, J.-Y., Rio, C., and Couvreux, F.: Deep Convection Triggering by Boundary Layer Thermals. Part II: Stochastic Triggering Parameterization for the LMDZ GCM, *Journal of the Atmospheric Sciences*, 71, 515–538, [https://doi.org/10.1175/JAS-D-12-](https://doi.org/10.1175/JAS-D-12-0337.1)
- 645 0337.1, publisher: American Meteorological Society Section: Journal of the Atmospheric Sciences, 2014b.
- Rochetin, N., Couvreux, F., and Guichard, F.: Morphology of breeze circulations induced by surface flux heterogeneities and their impact on convection initiation, *Quarterly Journal of the Royal Meteorological Society*, 143, 463–478, <https://doi.org/10.1002/qj.2935>, eprint: <https://onlinelibrary.wiley.com/doi/pdf/10.1002/qj.2935>, 2017.
- Sabater, S., Eloise, A., Feio, M. J., Gómez, R., Graça, M. A. S., Muñoz, I., Pardo, I., and Romaní, A. M.: Chapter 4 - The Iberian rivers, in: *Rivers of Europe (Second Edition)*, edited by Tockner, K., Zarfl, C., and Robinson, C. T., pp. 181–224, Elsevier, ISBN 978-0-08-102612-0, <https://doi.org/10.1016/B978-0-08-102612-0.00004-3>, 2022.
- 650 Sacks, W. J., Cook, B. I., Buening, N., Levis, S., and Helkowski, J. H.: Effects of global irrigation on the near-surface climate, *Clim Dyn*, 33, 159–175, <https://doi.org/10.1007/s00382-008-0445-z>, 2009.
- Schneider, U., Becker, A., Finger, P., Rustemeier, E., and Ziese, M.: GPCC Full Data Monthly Product Version 2020 at 0.25°: Monthly Land-Surface Precipitation from Rain-Gauges built on GTS-based and Historical Data, https://doi.org/10.5676/DWD_GPCC/FD_M_V2020_025, 2020.
- 655 Seneviratne, S. I., Corti, T., Davin, E. L., Hirschi, M., Jaeger, E. B., Lehner, I., Orlowsky, B., and Teuling, A. J.: Investigating soil moisture–climate interactions in a changing climate: A review, *Earth-Science Reviews*, 99, 125–161, <https://doi.org/10.1016/j.earscirev.2010.02.004>, 2010.
- 660 Seneviratne, S. I., Wilhelm, M., Stanelle, T., Hurk, B., Hagemann, S., Berg, A., Cheruy, F., Higgins, M. E., Meier, A., Brovkin, V., Claussen, M., Ducharne, A., Dufresne, J., Findell, K. L., Ghattas, J., Lawrence, D. M., Malyshev, S., Rummukainen, M., and Smith, B.: Impact of soil moisture-climate feedbacks on CMIP5 projections: First results from the GLACE-CMIP5 experiment, *Geophys. Res. Lett.*, 40, 5212–5217, <https://doi.org/10.1002/grl.50956>, 2013.



- Siebert, S. and Döll, P.: Quantifying blue and green virtual water contents in global crop production as well as potential production losses without irrigation, *Journal of Hydrology*, 384, 198–217, <https://doi.org/10.1016/j.jhydrol.2009.07.031>, 2010.
- Siebert, S., Burke, J., Faures, J. M., Frenken, K., Hoogeveen, J., Döll, P., and Portmann, F. T.: Groundwater use for irrigation – a global inventory, *Hydrology and Earth System Sciences*, 14, 1863–1880, <https://doi.org/10.5194/hess-14-1863-2010>, publisher: Copernicus GmbH, 2010.
- Taylor, C. M., Gounou, A., Guichard, F., Harris, P. P., Ellis, R. J., Couvreur, F., and De Kauwe, M.: Frequency of Sahelian storm initiation enhanced over mesoscale soil-moisture patterns, *Nature Geosci*, 4, 430–433, <https://doi.org/10.1038/ngeo1173>, publisher: Nature Publishing Group, 2011.
- Taylor, C. M., de Jeu, R. A. M., Guichard, F., Harris, P. P., and Dorigo, W. A.: Afternoon rain more likely over drier soils, *Nature*, 489, 423–426, <https://doi.org/10.1038/nature11377>, number: 7416 Publisher: Nature Publishing Group, 2012.
- Udina, M., Peinó, E., Polls, F., Mercader, J., Guerrero, I., Valmassoi, A., Paci, A., and Bech, J.: Irrigation impact on boundary layer and precipitation characteristics in Weather Research and Forecasting model simulations during LIAISE-2021, *Quarterly Journal of the Royal Meteorological Society*, 150, 3251–3273, <https://doi.org/10.1002/qj.4756>, _eprint: <https://onlinelibrary.wiley.com/doi/pdf/10.1002/qj.4756>, 2024.
- Vignon, E., Hourdin, F., Genthon, C., Van de Wiel, B. J. H., Gallée, H., Madeleine, J.-B., and Beaumet, J.: Modeling the Dynamics of the Atmospheric Boundary Layer Over the Antarctic Plateau With a General Circulation Model, *Journal of Advances in Modeling Earth Systems*, 10, 98–125, <https://doi.org/10.1002/2017MS001184>, _eprint: <https://onlinelibrary.wiley.com/doi/pdf/10.1002/2017MS001184>, 2018.
- Vogt, J., Soille, P., De, J. A., Rimaviciute, E., Mehl, W., Foisneau, S., Bodis, K., Dusart, J., Paracchini, M.-L., Haastруп, P., and Bamps, C.: A pan-European River and Catchment Database, <https://doi.org/10.2788/35907>, iSBN: 9789279069413 ISSN: 1018-5593, 2007.
- Wei, J. and Dirmeyer, P. A.: Dissecting soil moisture-precipitation coupling, *Geophysical Research Letters*, 39, <https://doi.org/10.1029/2012GL053038>, _eprint: <https://onlinelibrary.wiley.com/doi/pdf/10.1029/2012GL053038>, 2012.
- Wei, J., Dirmeyer, P. A., Wissler, D., Bosilovich, M. G., and Mocko, D. M.: Where Does the Irrigation Water Go? An Estimate of the Contribution of Irrigation to Precipitation Using MERRA, <https://doi.org/10.1175/JHM-D-12-079.1>, section: *Journal of Hydrometeorology*, 2013.
- Yamada, T.: Simulations of Nocturnal Drainage Flows by a q2l Turbulence Closure Model, *Journal of the Atmospheric Sciences*, 40, 91–106, [https://doi.org/10.1175/1520-0469\(1983\)040<0091:SONDFB>2.0.CO;2](https://doi.org/10.1175/1520-0469(1983)040<0091:SONDFB>2.0.CO;2), publisher: American Meteorological Society Section: *Journal of the Atmospheric Sciences*, 1983.
- Yamazaki, D., Ikeshima, D., Sosa, J., Bates, P. D., Allen, G. H., and Pavelsky, T. M.: MERIT Hydro: A High-Resolution Global Hydrography Map Based on Latest Topography Dataset, *Water Resources Research*, 55, 5053–5073, <https://doi.org/10.1029/2019WR024873>, _eprint: <https://onlinelibrary.wiley.com/doi/pdf/10.1029/2019WR024873>, 2019.
- Yang, Z., Dominguez, F., Zeng, X., Hu, H., Gupta, H., and Yang, B.: Impact of Irrigation over the California Central Valley on Regional Climate, <https://doi.org/10.1175/JHM-D-16-0158.1>, section: *Journal of Hydrometeorology*, 2017.
- Yao, Y., Schanke Aas, K., Arboleda Obando, P., Bentsen, M., Chen, L., Cook, B., Devaraju, N., Ducharne, A., Gosling, S., Hartley, A., Jägermeyr, J., Jones, C., Kim, H., Lawrence, D., Lawrence, P., Leung, R., Lo, M.-H., and McDermid, S.: Irrigation-expansion-induced impacts model-intercomparison project (IRRMIP), pp. EGU–14 584, <https://doi.org/10.5194/egusphere-egu23-14584>, conference Name: EGU General Assembly Conference Abstracts ADS Bibcode: 2023EGUGA..2514584Y, 2023.



705

Yao, Y., Ducharne, A., Cook, B. I., de Hertog, S. J., Aas, K. S., Arboleda-Obando, P. F., Buzan, J., Colin, J., Costantini, M., Decharme, B., Lawrence, D. M., Lawrence, P., Leung, L. R., Lo, M.-H., Narayanappa, D., Wieder, W., Wu, R.-J., Zhou, T., Jaegermeyr, J., Mcdermid, S., Pokhrel, Y., Elling, M., Hanasaki, N., Muñoz, P., Nazarenko, L., Otta, K., Satoh, Y., Yokohata, T., Jin, L., Wang, X., Mishra, V., Ghosh, S., and Thiery, W.: Impacts of irrigation expansion on moist-heat stress: first results from IRRMIP, <https://doi.org/10.21203/rs.3.rs-4835411/v1>, 2024.

Zou, X., Wang, G., Hagan, D. F. T., Li, S., Wei, J., Lu, J., Qiao, Y., Zhu, C., Ullah, W., and Yeboah, E.: Precipitation Sensitivity to Soil Moisture Changes in Multiple Global Climate Models, *Atmosphere*, 14, 1531, <https://doi.org/10.3390/atmos14101531>, number: 10 Publisher: Multidisciplinary Digital Publishing Institute, 2023.